UNDERSTANDING THE EFFECT OF MEASUREMENT TIME ON DRUG CHARACTERIZATION

by

HOPE E MURPHY

Bachelor of Science, 2016
Utica College
Utica

Submitted to the Graduate Faculty of the
College of Science and Engineering
Texas Christian University
in partial fulfillment of the requirements
for the degree of

Master of Science

December 2018

ACKNOWLEDGEMENTS

I would like to thank my research mentor Dr. Hana Dobrovolny for everything she has done to help with the completion of my masters. I would also like to thank the Physics and Astronomy department for funding me through my teaching assistantship. I would like to thank my family for their support during my master. I am grateful that my family has been there for me and has helped me succeed.

Contents

List of Figures

List of Tables

Abbreviations

AIC_C- Akaike information criterion with a correction for small sample sizes
Dox - Doxorubicin
$\varepsilon_{\max}$- Maximum efficacy
GI-101A xenograft - metastatic breast tumor xenograft
HeLa - Cervical cancer cells
HEK-293 - Human embryonic kidney cells
IC_{50}- Half maximal inhibitory concentration
MCF-7 - Breast cancer cells
ODE - Ordinary differential equations
RDE - Relative drug effect
SSR - Sum of squared residuals

Chapter 1

Introduction

1.1 Background

Cancer is a leading cause of death. This places a heavy burden on the health care system due to the chronic nature of the disease and the side effects caused by many of the treatments (1, 2, 3). Much research effort is spent improving the efficiency of current treatments (4) and on developing new treatment modalities (5, 6, 7, 8, 9). Diagnosis and treatment of cancer can be medically and technically complex (10). As cancer treatment becomes more personalized, mathematical models help to predict the time course of the tumor and optimize treatment regimens (11, 12).

There are two important quantities that characterize the effect of the drug: the maximum possible effect of a drug ($\varepsilon_{\max}$), and the drug concentration where the effect diminishes by half (IC_{50}). This work is intended to characterize the efficiency of anticancer drug treatments and develop a better way to measure $\varepsilon_{\max}$ and IC_{50} before treating patients to get the most effective therapeutic treatment for patients. This is an

important and useful goal because one day it could be used on patients in hospitals to improve the way IC_{50} and ε_{max} is measured when determining the amount of drugs to give cancer patients for the most effective treatment. If it is possible to predict the best dose of medicine for multiple lines of cells and predict the growth curve of the number of cells, then this research can be used to better understand tumors in cancer patients and to optimize personalized chemotherapy drug doses.

1.2 Cancer

Cancer is a disease that is characterized by the uncontrolled division of abnormal cells due to an abnormality in the growth control gene (13, 14). Non-cancerous cells only create more cells when they are needed by the body (15). These cells die after dividing a certain number of times and then get replaced with new cells. Cells are normally equipped with safeguards that keep the cells from having flawed copies of the cell or creating an excessive number of duplicate cells (15). These safeguards are lacking in cancer cells.

The abnormal cells are able to invade and metastasize in the body, while normal cells do not cause tissue invasion (16, 14). Ninety percent of cancer-related deaths are caused by metastasis. During metastasis, cancer cells relocate from the initial tumor to organs in other parts of the body first. The cells then start to form tumors in the organ to which the cells migrated (17).

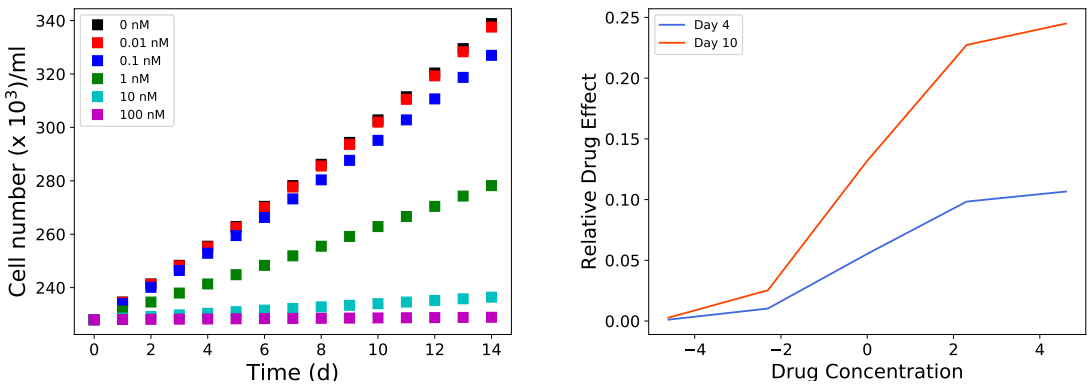

Figure 1.1: Computationally simulated data when plotting the Cell number / mL vs. Time with the cells being treated by various drug concentrations is shown on the left. The error bars for this figure are smaller than the size of the data points. The figure for the corresponding dose-response curves for day 4 and day 10 is on the right.

1.3 Cancer Treatment Efficacy

Unfortunately, the measured IC_{50}, as well as measured $\varepsilon_{\max}$, depend on the exact day that is chosen to make the measurement (18). The current method to find drug effect uses dose-response curves. Dose-response curves are created by counting cells in a lab. When counting cells in a lab cancerous cells are placed in 12-well plates and the number of cells is counted from a different well each day to understand how fast the cells grow. 12-well plates only have cancerous cells in each well because only one type of cells are put in the plate so we are able to assume that all of the cells that are counted are cancerous cells. A chosen concentration of drug is placed in each of the 12-well plates with the cells. On day zero the cells in each of the 12-well plates are treated with the chosen concentration of drug. The number of cells is counted each day. These measurements are used to determine the relative drug effect. The cell counts in the presence of different doses of drugs are used to generate the dose-response curve. Figure 1.1 (left) shows an

example of what experimental growth of cells would look like if the number of cells is counted every day for fourteen days when cells are treated with 0, 0.01, 0.1, 1, 10, and 100nM of drug. This data was computationally simulated. The black dots in the figure are mostly hidden behind the red dots because treating the cells with 0.01 nM of drug minimally reduces the number of cells. This data is used to create the dose-response curves that are used to measure IC_{50} and $\varepsilon_{\max}$. The dose-response curves are sigmoidal shaped and are used to extract the time-dependent parameters, IC_{50} and $\varepsilon_{\max}$. The shape of the dose-response curve changes depending on what day the values are measured. This can be seen in Figure 1.1 (right). The drug effect for day 4 shows a smaller relative drug effect than for day 10. The time point that is chosen to take the measurement for the volume of the tumor affects the value that will be measured for the effectiveness of the drug. This inaccuracy leads to a time-dependent bias. Two possible reasons for this error are due to the initial exponential growth and drug effect stabilization delays (19).

1.4 Mathematical Models

Mathematical models are used in a number of ways to help understand and treat cancer. Models are used to understand how cancer develops (20) and grows (21, 22, 23, 24). They are used to optimize (25, 26) or even personalize (27, 28, 12) current treatment regimens; predict the efficacy of new treatments (29) or combinations of different therapies (30, 31, 32); and give insight into the development of resistance to treatment (33, 34). While models have great potential to improve development and implementation of cancer treatment, they will only realize this potential if they provide accurate predictions.

The basis of any mathematical model used to study treatment of cancer is a model of tumor growth. This paper focuses on ordinary differential equation (ODE) models of tumor growth. A number of ODE models have been proposed to represent tumor growth (35, 36) and are regularly used to make predictions about the efficacy of cancer treatments (37). Unfortunately, choice of a growth model is often driven by ease of mathematical analysis rather than whether it provides the best model for growth of a tumor (35).

Some researchers have attempted to find the "best" ODE growth model by fitting various models to a small number of experimental data sets of tumor growth (38, 39, 40, 41). Taken altogether, the results are rather inconclusive, with results suggesting that choice of growth model depends at least in part on the type of tumor (39, 40). This leaves modelers with little guidance in choosing a tumor growth model.

Early studies of tumor growth were concerned with finding equations to describe the growth of cancer cells (21, 22, 23, 24) and many of the models examined here were proposed at that time. The models predict the growth of a tumor by describing the change in tumor volume, V, over time. The model equations used in this analysis and the models are described below. The parameters a, b, and c can be adjusted to describe a particular data set.

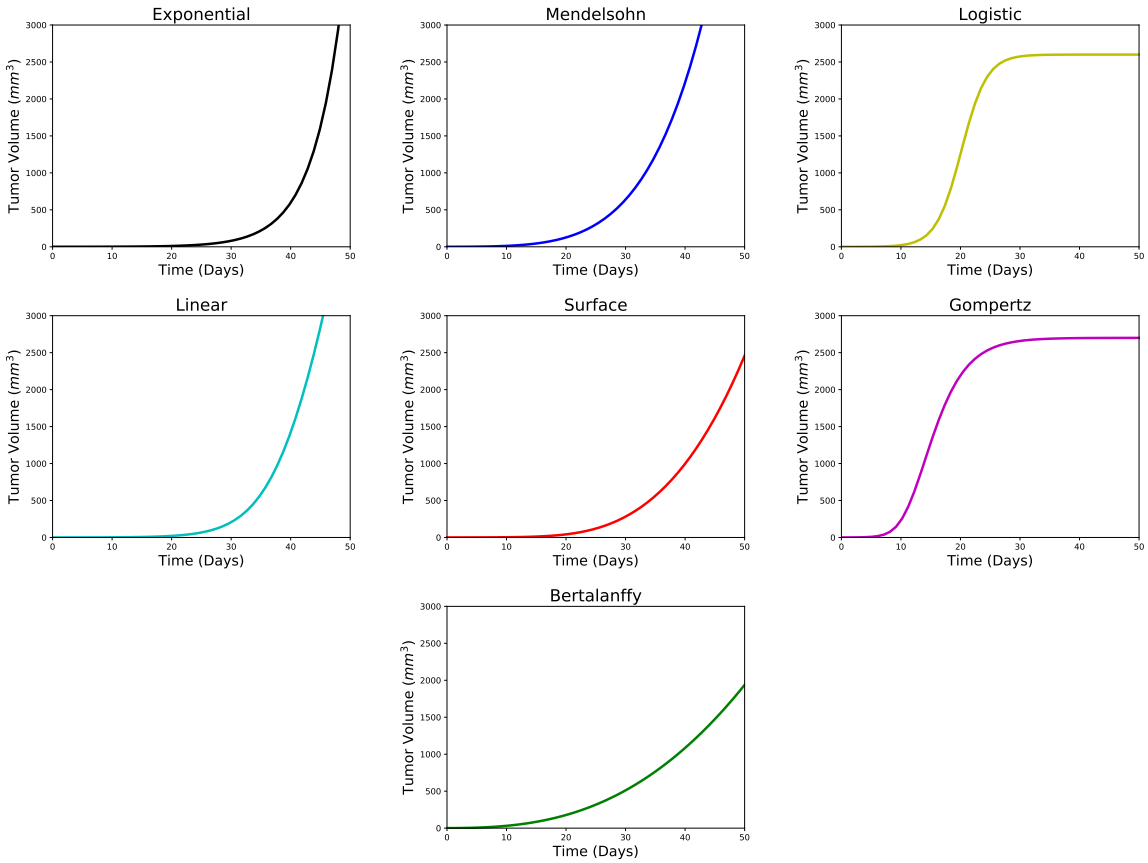

Figure 1.2: These graphs show the shape of the seven models that will be used. The exponential, Mendelsohn, linear, and surface model are biologically unrealistic. These models work well for the initial growth, but the growth should level off to account for cells running out of space and nutrients. The logistic, Bertalanffy, and Gompertz models are more biologically realistic models that predict early growth and late growth suppression.

Exponential:

$$\frac{dV}{dt} = aV(t) \tag{1.1}$$

In the early stages of tumor growth, cells divide regularly, creating two daughter cells each time. A natural description of the early stages of cancer growth is thus the exponential model (42), where growth is proportional to the population. The proportionality constant a is the growth rate of the tumor. The exponential model predicts the perfect scenario when cell growth continuously doubles due to cells not having any constraints. But, in the body cells are limited to the amount of resources that are available because cells are limited to the amount of oxygen, nutrients and space that is available to the cancer cells (43). This model was often used in early analysis of tumor growth curves (21, 22, 23, 24) and appears to work quite well at predicting early growth. It is known to fail, however, at later stages when angiogenesis and nutrient depletion begin to play a role (35, 40).

Mendelsohn: A generalization of the exponential growth model was introduced by Mendelsohn (44). Similar to the exponential model, the proportionality constant a is the growth rate of the tumor. In this model, growth is proportional to some power, b, of the population. This model reduces to an exponential equation when b equals 1 (43).

$$\frac{dV}{dt} = aV(t)^b \tag{1.2}$$

Logistic: The logistic (or Pearl-Verhulst) equation was created by Pierre Francois Verhulst in 1838 (45). This model describes the growth of a population that is limited by

a carrying capacity of b. When using this model to describe tumor growth, the carrying capacity describes the amount of space and nutrients that is available for the tumor. Biologically, this means that a tumor will stop growing when it runs out of space in an organ or the tumor runs out of oxygen or other nutrients to enable the cells to divide.

$$\frac{dV}{dt} = aV(t)(1 - \frac{V(t)}{b}) \tag{1.3}$$

The logistic equation can explain the decrease in tumor growth and the mass of the tumor reaches an asymptote, by assuming that the growth rate (a) decreases linearly with the size until it equal to zero at the carrying capacity (b), with the model being symmetric.

Linear: The linear model assumes initial exponential growth that changes to growth that is constant over time. The volume of a tumor grows linearly. This means that the radius grows at a rate of $t^{\frac{1}{3}}$ and the linear model assumes that growth is constant.

$$\frac{dV}{dt} = \frac{aV(t)}{(V(t) + b)} \tag{1.4}$$

The model was used to model growth of bacterial colonies in a culture, so we thought it would be a good model to show the growth of tumors in a dish because you are measuring the area of the tumor instead of the volume. This model might not work for spherical tumors because for spherical tumors the volume is measured instead of the area. In our formulation of the model, the initial exponential growth rate is given by a/b and the later constant growth is a. The model was used in early research to analyze growth of cancer cell colonies (24).

Surface: The surface model assumes only a thin layer of cells at the surface of the tumor are dividing while the cells inside the solid tumors do not reproduce; they are mitotically inactive (46). Our formulation again assumes exponential growth (a) at early times with the surface growth ($a/b^{1/3}$) taking over at longer times. The model assumes that surface growth occurs at an exponential rate, where the denominator takes into account that the tumor is spherical in shape.

$$\frac{dV}{dt} = \frac{aV(t)}{(V(t)+b)^{\frac{1}{3}}} \tag{1.5}$$

This model cannot account for the long-term growth of cancer cells because there is a reduction in growth rate and then blood vessels are formed during the process of vascularization (35).

Bertalanffy: The Bertalanffy equation was created by Ludwig Bertalanffy as a model for organism growth (47). This model assumes that growth occurs proportional to surface area, but that there is also a decrease of tumor volume due to cell death. The growth of the tumor occurs at a rate of $aV(t)^{\frac{2}{3}}$. The decrease of tumor volume due to cell death occurs in proportion to the volume of the tumor with constant b. This cell death occurs at an exponential rate.

$$\frac{dV}{dt} = aV(t)^{\frac{2}{3}} - bV(t) \tag{1.6}$$

The curve is sigmoid in shape. It both matches the curves of experimental tumor growth and the derivation meets the biologically meaningful parameters. This model was shown to provide the best description of human tumor growth (38).

Gompertz: Benjamin Gompertz originally created the Gompertz model in 1825 in order to explain human mortality curves (48). The cells in a tumor are not all dividing but the cells that divide, are dividing at a rate that is similar to the early stages. The decaying growth rate is based on how all of the cancer cells in the tumor are growing and assumes an exponential decaying growth rate. The growth rate equals zero when $\frac{b}{(V(t)+c)} = 1$ because $\ln 1 = 0$ (35). This term describes the decaying growth rate.

$$\frac{dV}{dt} = aV(t) \ln \frac{b}{(V(t) + c)} \tag{1.7}$$

The model is a generalization of the logistic model with a sigmoidal curve that is asymmetrical with the point of inflection. The curve was eventually applied to model growth in size of entire organisms (49) and more recently, was shown to provide the best fits for breast and lung cancer growth (40). This model is the most applied model when describing tumor growth curves because it predicts the behavior of the tumor most accurately and over longer periods of time and fits how the plots are close to being straight lines (35).

1.5 Questions to Answer

1. How does model choice affect the predicted IC_{50} and $\varepsilon_{\max}$?

Many researchers realize that improper choice of growth model is problematic (35) and can lead to differences in predictions of treatment outcomes (36, 37). One study compared and quantified differences in predictions of the various models and how these differences affect predictions of tumor growth (50). In this paper, we present results of

analysis of the various ODE growth models highlighting their predictions of tumor growth in the presence of chemotherapy, focusing on estimates of IC_{50} and ε_{max} produced by the different models.

2. Can a better way to measure IC_{50} and ε_{max} be found using mathematical modeling?

In order to determine correct dosage of chemotherapy drugs, the effect of the drug must be properly quantified. There are two important quantities that characterize the effect of the drug: ε_{max} is the maximum possible effect of a drug, and IC_{50} is the drug concentration where the effect diminishes by half. The drug effect curves depend on measurement time, so the estimated IC_{50} and ε_{max} also depend on measurement time. The objective of my research is to use mathematical modeling to test a new method for measuring ε_{max} and IC_{50} that gives estimates independent of measurement time.

Chapter 2

Modeling of Drug Treatment Assays

2.1 Introduction

Early studies of tumor growth were concerned with finding equations to describe the growth of cancer cells (21, 22, 23, 24) and many of the models examined here were proposed at that time. The seven models used are exponential, Mendelsohn, logistic, linear, surface, Bertalanffy, and Gompertz. Four of the models (exponential, Mendelsohn, linear, and surface) predict indefinite growth of the tumor, but the remaining three models predict finite tumor sizes. The seven models will be used in this chapter to describe how choice of model affects the predicted IC_{50} and $\varepsilon_{\max}$ values.

2.2 Methods

To get a comprehensive analysis, seven ODE models will be used. The models predict the growth of a tumor by describing the change in tumor volume, V, over time. Parameters

a, b, and c can be adjusted to describe a particular data set. We describe the analysis of the logistic model in detail as an example to guide the reader through the analysis.

The models are simulated using the parameter values from Fig. 3 in (50), presented in Table 2.1. The parameter values were estimated using data from Worschech et al. (51) of a GI-101A xenograft in nude mice (Figure 1A of (51), control data). The GI-101A xenograft is implanted under the skin of the nude mouse causing the tumor to grow directly under the skin. This allows researchers to see the tumor grow and differentiate between what is the tumor and what is normal tissue in the mouse. When measuring the volume of the tumor a caliper would have been used. To measure the width of tumor the jaws on the caliper would have been lightly closed onto the tumor to make an accurate measurement. This would have been used to measure the size of the tumor in order to determine the volume of the tumor. The tumor is not perfectly circular so the measured volume will not be totally accurate, leading to some error in the measurements. The caliper has an error of 0.05 mm. The data was extracted using WebPlotDigitizer, an online data extraction tool. Fitting was performed by minimizing the sum of squared residuals (SSR),

$$\mathrm{SSR} = \sum_i (x_i - m_i)^2, \tag{2.1}$$

where x_i are the experimental data points, and m_i are the predicted model values at the same times. The lowest SSR was found using the Python Scipy `fmin_tnc` function, which uses a truncated Newton algorithm. The best fit was be determined by minimizing the SSR and the best model was determined by AIC_C.

Model	a	b	c
Exponential	0.0246 /d		
Mendelsohn	0.105 /d	0.785	
Logistic	0.0295 /d	6920 mm^3	
Linear	132 mm^3/d	4300 mm^3	
Surface	0.291 mm/d	708 mm^3	
Gompertz	0.0919 /d	15500 mm^3	10700 mm^3
Bertalanffy	0.306 mm/d	0.0119 /d	

Table 2.1: Parameters for the seven ODE models. The parameter values are from Fig. 3 in (50).

Model		a	b	c
Exponential	25th	0.00828 /d		
	95th	0.0254 /d		
Mendelsohn	25th	0.0266 /d	0.715	
	95th	0.138 /d	0.969	
Logistic	25th	0.0136 /d	325 mm^3	
	95th	2.53 /d	$85,368$ mm^3	
Linear	25th	33.4 mm^3/d	14.9 mm^3	
	95th	$1,095$ mm^3/d	$28,896$ mm^3	
Surface	25th	0.0757 mm/d	23.6 mm^3	
	95th	0.640 mm/d	$20,100$ mm^3	
Gompertz	25th	0.0144 /d	$2,320$ mm^3	27.7 mm^3
	95th	89,062 /d	$4,419,058,288$ mm^3	$4,419,056,146$ mm^3
Bertalanffy	25th	0.167 mm/d	0.00066 /d	
	95th	0.554 mm/d	0.0447 /d	

Table 2.2: The 95 percent confidence intervals for the parameters for the seven ODE models. The parameter values are from Fig. 3 in (50).

Estimated error was completed using the percentile bootstrap method for parameters a and b. Fit residuals were sampled with replacement to create 1,000 bootstrap replicates of the data sets. Then a 95% confidence interval was estimated using these data sets. A 95% confidence interval means that after putting the data set in numerical order and we want to look at the 25th and the 975th values. The values were sorted using the sort function in Excel. The confidence interval values can be found in Table 2.2.

2.2.1 Implementing Drug Effect

We examined how predictions differed when chemotherapy was added to the models. This is particularly important since growth models are often used as a basis for predicting the efficacy of cancer therapies.

To understand how the drug affects the growth of tumor cells, we use the drug efficacy, ϵ. ϵ is given by

$$\epsilon = \frac{\varepsilon_{\max} D}{D + \mathrm{IC}_{50}}, \tag{2.2}$$

where D is the drug concentration, $\varepsilon_{\max}$ is the maximum possible effect of a drug, and IC_{50} is the drug concentration where the effect diminishes by half. We assume that the drug is given on day one and a constant concentration of drug is applied to the cancerous tumor. ϵ, gives the relative reduction in a particular property where $\epsilon = 0$ means that there is no effect and $\epsilon = 1$ means 100% reduction. If we assume that the drug decreases growth rate, we multiply a by $(1 - \epsilon)$ to represent the effect of the drug in the model. If we assume that the drug decreases the carrying capacity, we multiply b by $(1 - \epsilon)$ to represent the effect of the drug in the model. For simulations, we assume that both $\varepsilon_{\max}$ and IC_{50} are 1. For $\varepsilon_{\max}$, this means we assume that we have a perfectly effective drug. For IC_{50}, this assumption is equivalent to expressing drug concentrations relative to IC_{50}.

2.2.2 Relative Drug Effect

Relative drug effect is defined as

$$R = 1 - \frac{V_{\text{drug}}}{V_{\text{no drug}}}, \tag{2.3}$$

where V_{drug} is the volume of the tumor remaining after drugs are applied to the cells and $V_{\text{no drug}}$ is the volume of the tumor when no drugs are applied to the cells.

To determine how IC_{50} and ε_{max} vary with measurement time, we look at the relative drug effect vs. $\log(D)$ measured on a particular day and find ε_{max} and IC_{50} for the drug effect curve on that day. The curves are all sigmoids, but clearly have different IC_{50} and ε_{max}. Curve fitting was used to solve for ε_{max} and IC_{50}. The best fit was determined by minimizing the SSR using the Python Scipy `curve_fit` function, which fits a sigmoid function to the data.

2.3 Results

2.3.1 Determining time-dependence of IC_{50} and ε_{max}

We use the logistic model to show how the time-dependence of IC_{50} and ε_{max} is calculated. Figure 2.1 shows the volume of the tumor as a function of time for several values of drug efficacy using the logistic model. The left graph models a drug that reduces growth rate while the right graph models a drug that reduces carrying capacity.

Experimentally, drug effect is measured as a function of the dose, so rather than plotting the number of cells as a function of efficacy, we look at the relative drug effect as

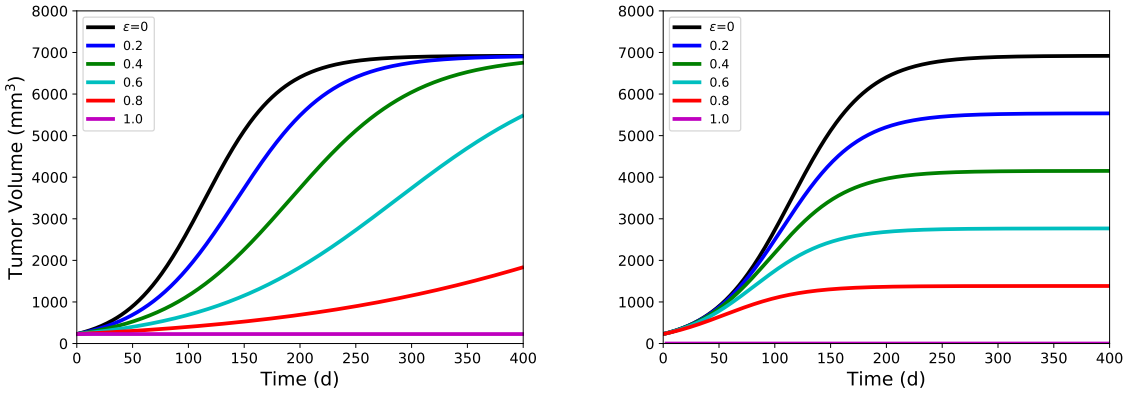

Figure 2.1: Reduce growth rate (left) and reduce maximum number of cells (right). Plotting Tumor Volume vs. Time where ϵ varies between 0 and 1.

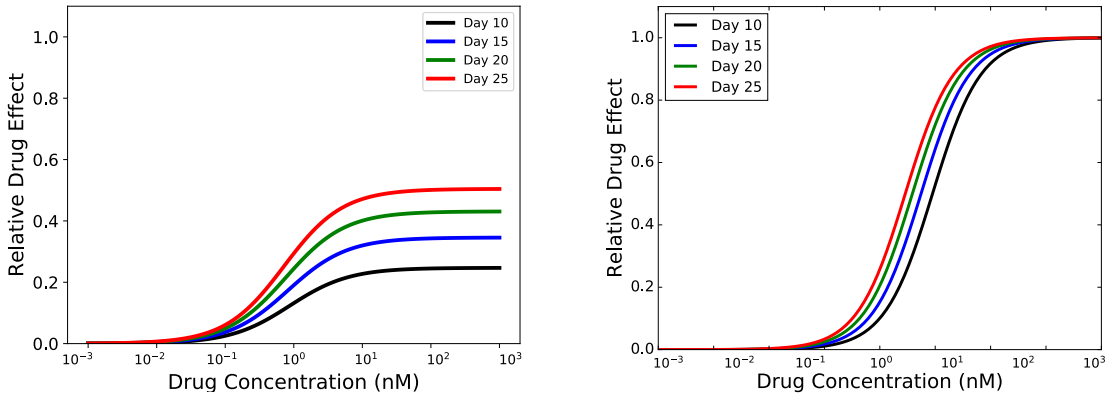

Days	$\varepsilon_{\max}$	IC_{50}
Day 10	0.247	0.873 nM
Day 15	0.346	0.817 nM
Day 20	0.431	0.767 nM
Day 25	0.504	0.720 nM

Days	$\varepsilon_{\max}$	IC_{50}
Day 10	1.038	5.722 nM
Day 15	1.034	3.765 nM
Day 20	1.032	2.848 nM
Day 25	1.030	2.477 nM

Figure 2.2: Logistic model, reduce a (left) and reduce b (right). Plotting $\log(D)$. $\varepsilon_{\max}$ and IC_{50} estimates for each measurement day are given in the table below the graph.

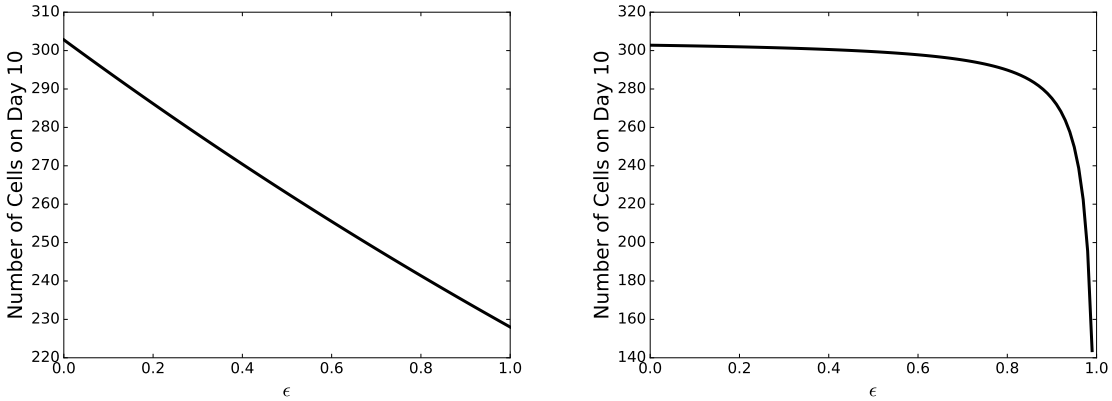

Figure 2.3: Reduce growth rate (left) and reduce maximum number of cells (right). Plotting Number of Cells on Day 10 vs. ϵ.

a function of the drug dose. We show several of these dose-response curves in Figure 2.2 for several measurement times. We see from Figure 2.2 (left) that $\varepsilon_{\max}$ and IC_{50} increase with increasing measurement time when the drug effect is applied to the growth rate. This is a problem because the day that is chosen to measure $\varepsilon_{\max}$ and IC_{50} causes there to be a different recommended dose for a patient. The table included in Figure 2.2 shows $\varepsilon_{\max}$ and IC_{50} calculated for drugs having an effect on growth rate. The table included in Figure 2.2 (right) shows $\varepsilon_{\max}$ and IC_{50} calculated for drugs having an effect on carrying capacity.

The largest difference between the relative drug effect on the growth rate and the relative drug effect on the carrying capacity is that $\varepsilon_{\max}$ increases with measurement time for a drug reduces growth rate but $\varepsilon_{\max}$ stays constant with measurement time for a drug that reduces carrying capacity. For both drugs depicted in Figure 2.2, IC_{50} decreases with time. We can get a more complete picture of the measurement time dependence of

both IC_{50} and $\varepsilon_{\max}$ by repeating the above procedure over a range of measurement times. We measured the relative drug effect over 50 days, using a time-step of 1 day.

When drugs are characterized in the lab, the reduction in tumor cells is measured on a particular day. For example, Figure 2.3 shows the number of cells on day 10 versus ϵ for the logistic model. Figure 2.3 (left) shows a negative linear relationship between the number of cells and ϵ when $(1-\epsilon)$ is applied to the growth rate. This graph starts with about 300 cells when ϵ is 0 and decreases to 228 cells when ϵ is equal to 1 because this is the initial number of cells. In Figure 2.3 (right), $(1-\epsilon)$ is applied to the carrying capacity, causing there to be a gradual decrease in the number of cells until around $\epsilon = 0.9$ when the number of cells drastically drops. The number of cells when ϵ is equal to 1 is much smaller for Figure 2.3 (right), where the number of cells is about 140 cells. We see that drugs with different mechanisms result in different responses as the dose is increased.

Figure 2.4 shows $\varepsilon_{\max}$ vs. days in order to show how the measured $\varepsilon_{\max}$ value is dependent on the day that the measurement is taken. In the top left figure, a drug acts on the growth rate (a) for the exponential, Mendelsohn, logistic, and Gompertz models. In this figure we see that $\varepsilon_{\max}$ increases. In the center figure in Figure 2.4, there is little change to $\varepsilon_{\max}$ when a drug acts on b in the logistic model with the largest decrease happening during the first 10 days.

Figure 2.4 shows that the curve steadily increases with a maximum value of 0.9 when the drug acts on a for the logistic, exponential, Mendelsohn, linear, surface, Bertalanffy, and Gompertz model. The curve also steadily increases when the drug acts on b for the Mendelsohn, linear, and surface model. In Figure 2.4, we see that the curve increases rapidly and then levels off at approximately 1 around day 10 when the drug acts on

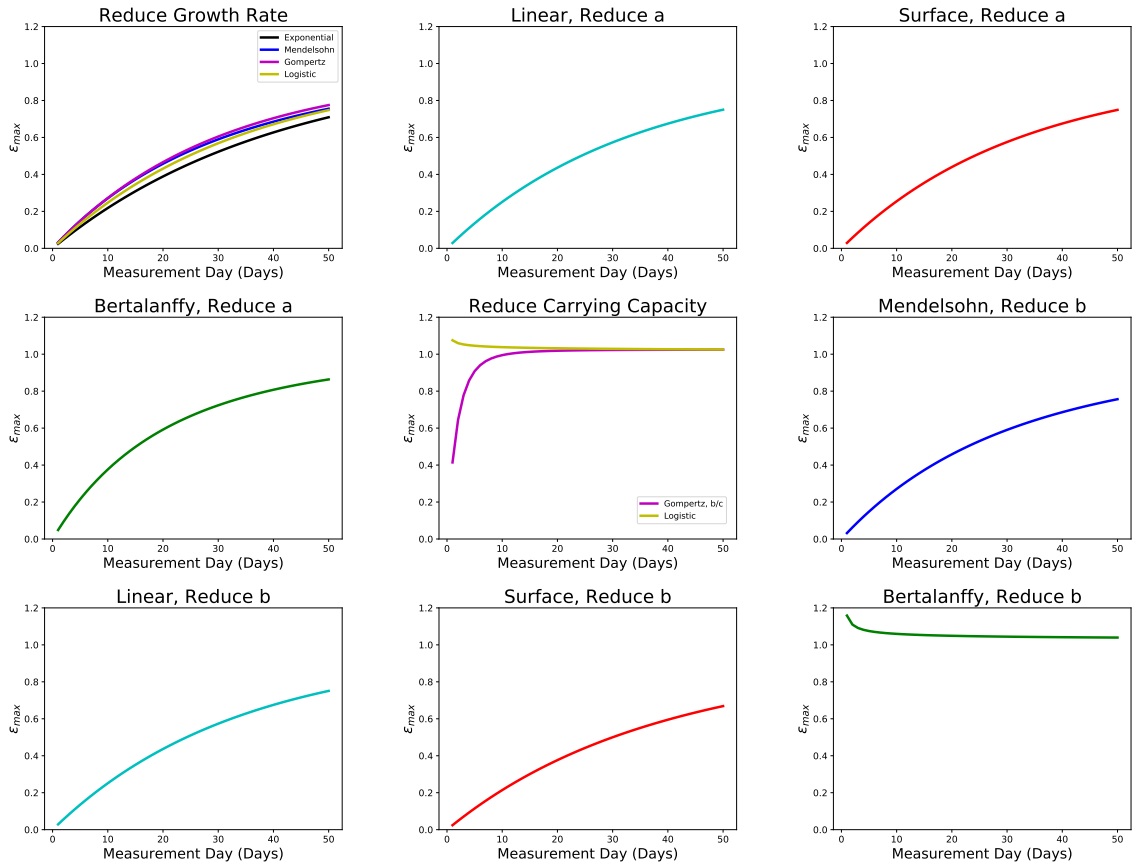

Figure 2.4: $\varepsilon_{\max}$ graphs for relative drug effect of all seven models.

either b or c for the Gompertz model in the center figure. Figure 2.4 shows that the curve decreases when the drug acts on b for the logistic and the Bertalanffy model where the $\varepsilon_{\max}$ values are all above 1.02 and are as high as 1.16. The correct value of $\varepsilon_{\max}$ in this case is 1, so we would hope that the measurement procedure returns this value of $\varepsilon_{\max}$. Figure 2.4 shows that the current experimental measurement technique almost never returns the correct value of $\varepsilon_{\max}$. The only exception is the Gompertz model.

Figure 2.5 shows drastic differences in IC_{50} values when measurements are taken on different days. The center panel in Figure 2.5 predicts that IC_{50} drastically decreases during the first 10 days for a drug that reduces the carrying capacity (b) in the logistic

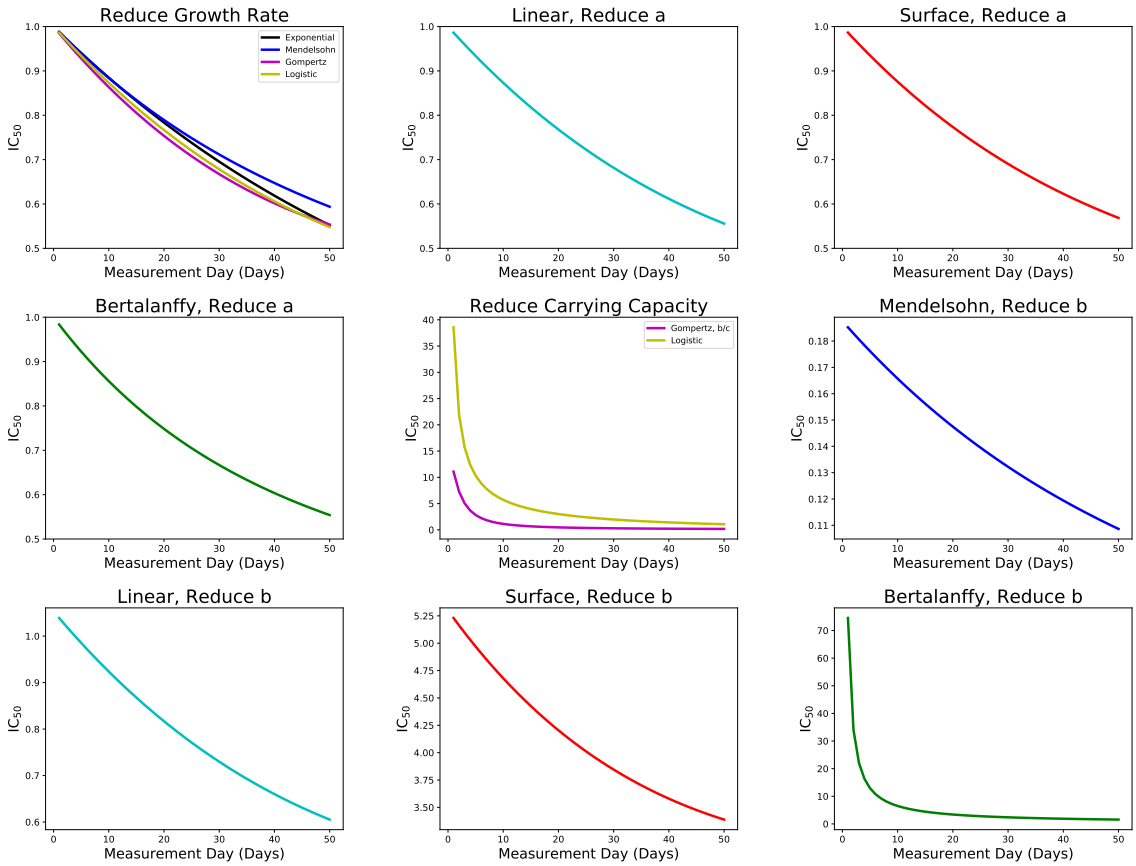

Figure 2.5: IC_{50} graphs for relative drug effect of all seven models.

model with IC_{50} values ranging from 0 to 40. The curve looks similar when the drug acts on b for the Bertalanffy model where the range of IC_{50} values is from 0 to 80. The center figure in Figure 2.5 predict that IC_{50} drastically decreases from 3 during the first 10 days for a drug that reduces b or c in the Gompertz model and drops down to about 0 by day 30. All of the other graphs in Figure 2.5 decrease steadily and estimate that IC_{50} is less than 1. The smallest values are predicted for the drug reducing b for the Mendelsohn and the linear model where the maximum values are 0.052 and 0.20 respectively. Simulations of the current experimental measurement technique do not return the expected value of IC_{50} for any measurement day, no matter which model is assumed.

2.3.2 Sensitivity Analysis

In order to assess how our results depend on model parameters, we did a sensitivity analysis by varying model parameters and re-running the simulations. Fig. 3 in (50), shows the best fits of all seven ODE tumor growth models to the data from Worschech et al. (51), while Fig. 1 in (50) shows the best fits of the ODE tumor growth models to the first half of the data from Worschech et al. (51). The parameter estimates varied between the two figures causing the need to complete a sensitivity analysis. The range that was chosen to complete the sensitivity analysis for each parameter was the range between the parameter estimates in Fig. 1 and Fig. 3 in (50).

Figures 2.6, 2.7, and 2.8 show the sensitivity analysis for the parameters in the models to show how choice of initial conditions changes the predicted $\varepsilon_{\max}$ and IC_{50} values. Due to the large number of graphs created to have a complete sensitivity analysis for all seven models, only some of the graphs are shown in this section. The remaining graphs are located in Figures A.10, A.11, A.12, and A.13.

Figures 2.6, 2.7, and 2.8 show each type of variation for the $\varepsilon_{\max}$ and IC_{50} values over time. Some of the graphs have very small differences in the variation caused by changing the initial parameter predictions and other graphs have large variations in the $\varepsilon_{\max}$ and IC_{50} values.

As seen in Figure 2.6, the smallest variation caused by changing initial parameter predictions occurred in the center graph and the bottom left graph when initial parameter a predictions are increased. Minimal variations can be seen in Figure 2.6 for the top left and the top right graphs, but in these graphs it can be seen that increasing initial

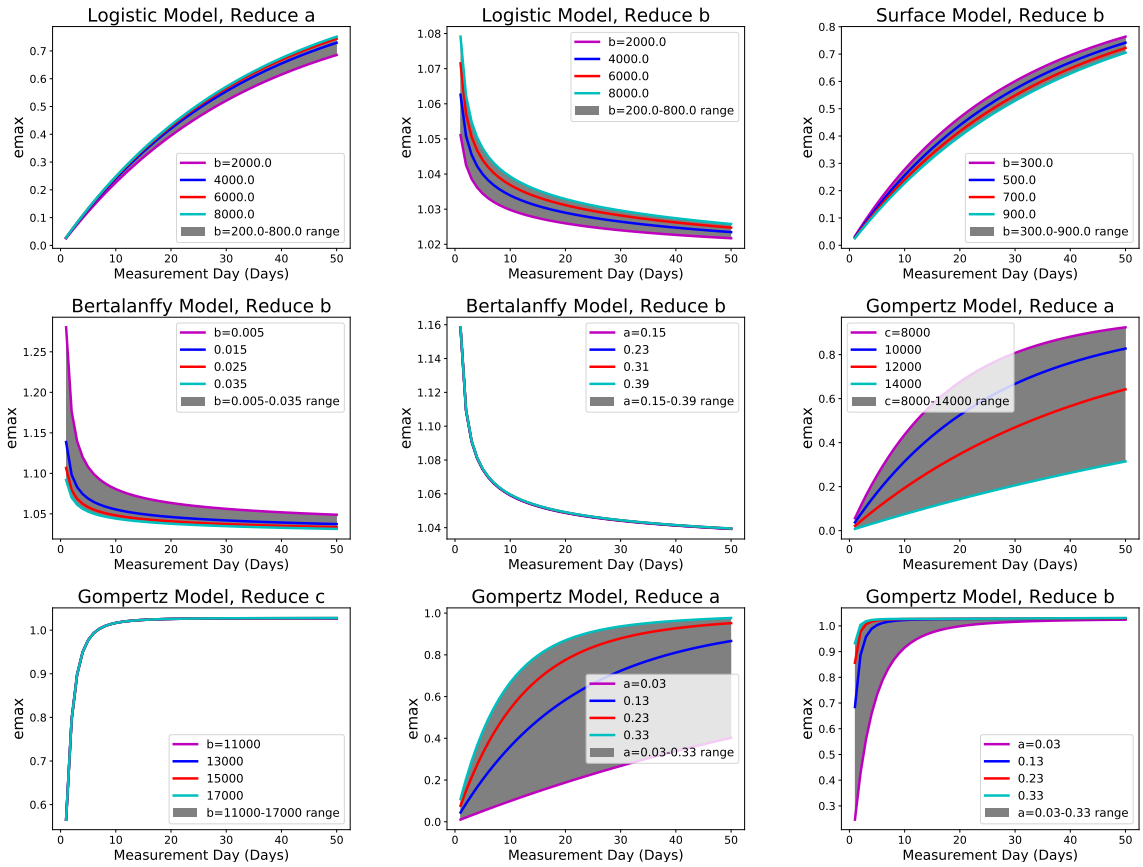

Figure 2.6: Sensitivity analysis for $\varepsilon_{\max}$ as a function of the measurement time, where the parameters for a, b, or c are varied.

predictions for parameter a have the opposite effect. There is also minimal variation in the top middle, middle left, and bottom right graphs with the most variation occurring at the inflection point. The graphs with the most variation in Figure 2.6 are the middle right and the bottom middle graph, where the curves predicted for IC_{50} values range from a parabolic shape to a line.

In Figure 2.7, the smallest variation can be seen in the center graph and the bottom left graph when initial parameter a predictions are increased. Minimal variations can also be seen in Figure 2.8 for the top middle and the top right graphs where the most variation occurs at the inflection point when the initial parameter for a is varied. The

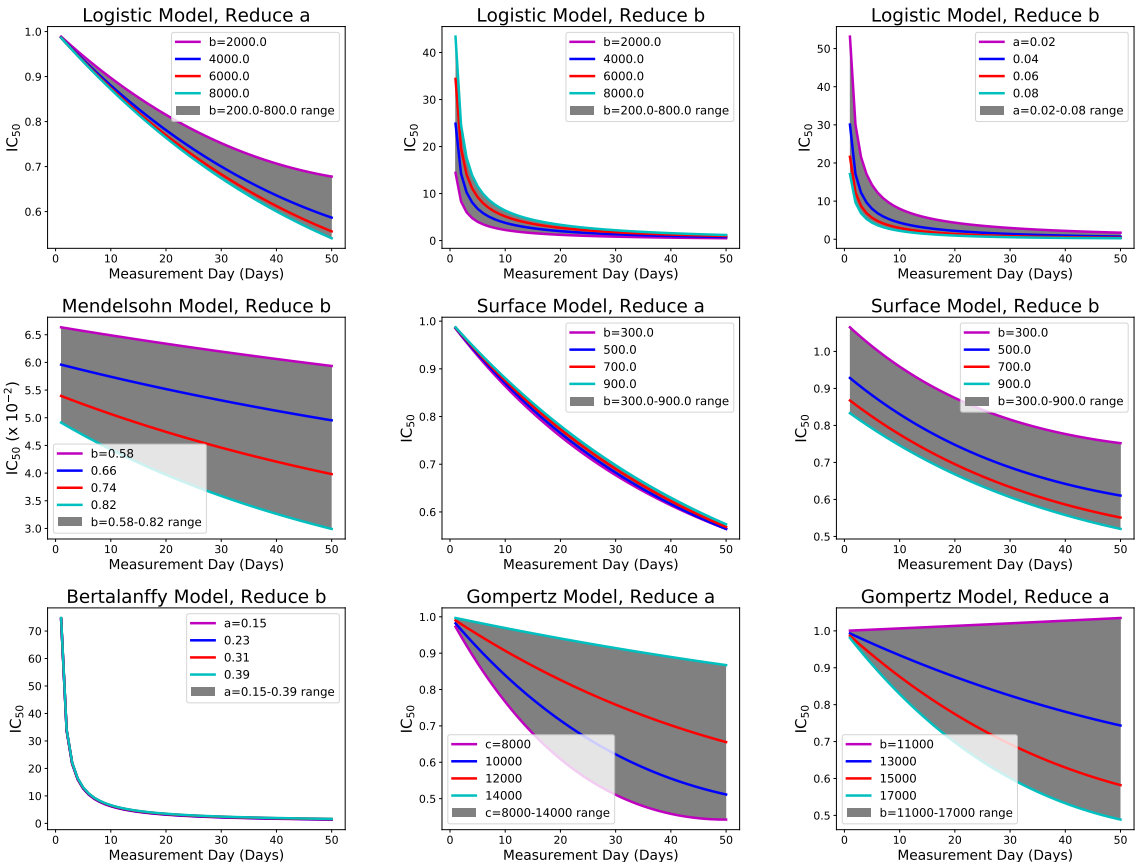

Figure 2.7: Sensitivity analysis for IC_{50} as a function of measurement time, where the parameters for a, b, or c are varied.

graphs with the most variation in Figure 2.7 are the middle left, the middle right, the bottom middle, and the bottom right graphs. It can be seen that the middle left and the middle right graphs have large differences in the predicted IC_{50} values, but minimal changes in the slope of the IC_{50} curves. For the bottom middle and the bottom right graphs in Figure 2.7 the curves predicted for IC_{50} values range from a parabolic shape to a line.

As seen in Figure 2.8, we found that the growth rate parameters caused the largest differences in the IC_{50} curves. The predicted curves for IC_{50} are parabolic for the highest growth rate values and become more linear as the growth parameters decreases for the

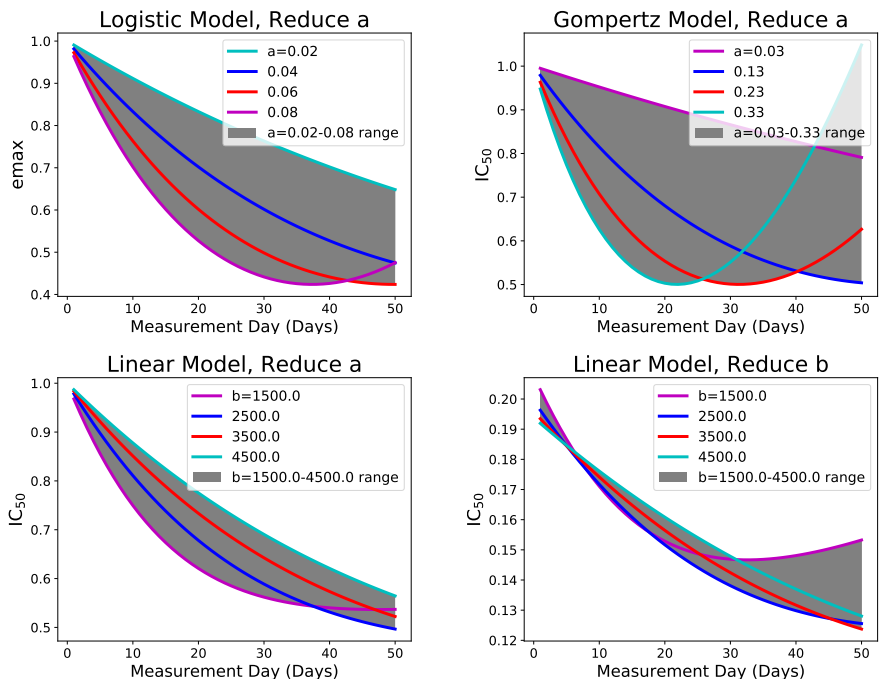

Figure 2.8: Sensitivity analysis for IC_{50} as a function of measurement time, where the growth rate parameters are varied. The graphs included in this figure show the largest variation due to changes in parameters.

top row of graphs. The opposite effect happens for the linear graphs that are presented in the bottom row of Figure 2.8.

2.4 Summary

The seven ODE models that we used predicted tumor growth by describing the change in tumor volume, V, over time. We examined how predictions differed when chemotherapy was added to the models to predict the efficacy of cancer therapies. We determined how IC_{50} and $\varepsilon_{\max}$ vary with measurement time by looking at the relative drug effect vs. $\log(D)$ measured on a particular day and finding $\varepsilon_{\max}$ and IC_{50} for the drug effect curve on that day. When drugs are characterized in the lab, the reduction in tumor cells is

measured on a particular day. We can got a complete picture of the measurement time dependence of both IC_{50} and ε_{max} by measuring over 50 days using mathematical models. Lastly, we assessed how our results depend on model parameters by doing a sensitivity analysis. We varied model parameters and found that some of the graphs had very small differences in the variation caused by changing the initial parameter predictions and other graphs had large variations in the ε_{max} and IC_{50} values. Our study indicates that the current technique for measuring IC_{50} and ε_{max} does not return the correct values of IC_{50} and ε_{max}. In fact, the measured values of IC_{50} and ε_{max} are strongly dependent on the day on which measurements are made with large deviations from the correct values on most measurement days.

Chapter 3

Extracting Drug Efficacy Parameters with Model Fitting

3.1 Introduction

$\varepsilon_{\max}$ and IC_{50} are important values to determine how much chemotherapy drugs are needed to treat a patient. However, when making experimental measurements $\varepsilon_{\max}$ is often not measured, meaning that IC_{50} is the value that is used to determine the dose of drug that patients should be given. When determining the values for $\varepsilon_{\max}$ and IC_{50} curves are generated that show the measured tumor volume on a certain day versus the drug dose (52). As seen in the previous chapter, the way IC_{50} and $\varepsilon_{\max}$ are currently measured is a problem because they depend on what day the values are measured (18). It is important to be able to determine IC_{50} and $\varepsilon_{\max}$ values that do not depend on the day that the values are measured to find more suitable doses when patients are being treated.

The objective of this chapter is to develop and test a method for estimating the drug efficacy parameters from tumor growth data. The essential role of this research is the development of a new modeling framework that will allow prediction of crucial treatment parameters that can be used to optimize therapeutic doses for more effective and safer cancer treatment. This work will make it possible to get a more complex understanding of the efficacy of a drug by estimating IC_{50} and $\varepsilon_{\max}$ values and providing time-independent values for these parameters.

3.1.1 Breast Cancer

The data used in this chapter to test our new method is from breast cancer. Breast cancer is one of the four major types of cancer, accounting for roughly 40 percent of cancer cases across the world. The four major types of cancer cause approximately 2.7 million deaths and at least 5 million people are diagnosed each year with one of these cancers (53). Breast cancer accounts for 12% of all cancers diagnosed worldwide each year for women and is the second most common cause of death from cancer for women. There is a 90% overall 5-year rate of survival for breast cancer with variations based on the stage of the disease (54).

The risk of having breast cancer increases if you have a family or personal history of breast cancer and inherit mutations in the BRCA1 and BRCA2 genes, which are genes that make someone susceptible to breast cancer (54). Treatment for breast cancer usually consists of surgery, and may be proceeded by chemotherapy, radiation therapy, or targeted therapy (54).

3.2 Methods

Data from (55) for 0 nM, 200 nM, 500 nM, and 1000 nM of doxorubicin in MCF-7 cells was extracted using WebPlotDigitizer, an online data extraction tool. MCF-7 cells are breast cancer cells. For an experiment like this MCF-7 cells would have been placed in a plate with multiple wells along with medium in order to give the cells the nutrients needed to grow. The cells in the wells would have been treated on day one of the experiment. Each day the number of cells would have been counted by counting from a different well each day. Each well starts out with approximately the same number of cells and the cells are from the same culture dish so we can assume that the cells grow at approximately the same rate. The largest error when counting cells comes from cells in the wells growing at different rates. At the end of the experiment it is possible for the number of cells to drastically decrease due to the cells running out of room in the well or not having enough medium to get nutrients from.

Fitting was performed by minimizing the sum of squared residuals (SSR),

$$\mathrm{SSR} = \sum_i (x_i - m_i)^2, \tag{3.1}$$

where x_i are the experimental data points, and m_i are the predicted model values at the same times. The lowest SSR was found using the Python Scipy `fmin_tnc` function, which uses a truncated Newton algorithm. A truncated Newton algorithm is used when there are multiple independent variables to optimize a non-linear function. The parameters of the function are determined by an iterative optimization algorithm that is applied repeatedly to approximately solve the equations. Initially an estimation of the parameter

values is given to the solver and then the inner solver updates the parameters of the function. A set number of repetitions is given to the algorithm to determine when the solver will be complete. The best approximation needs to be determined after a set number of repetitions. Bootstrapping using 1000 surrogate data sets was performed to estimate the error in the parameter values.

Cellular growth data is fit for each cell line in order to find the best fit. The control data is fit at the same time as cells in the presence of three different concentrations of drugs when the best parameter fit is being determined. The SSR is being used in order to determine the best fit.

The mathematical model that we have chosen to use is a logistic model because it fits the cell growth data the best. When we fit the data using a mathematical model of tumor growth, we examined two assumptions for the effect of doxorubicin: first assuming that doxorubicin reduces growth rate, and second assuming that it reduces the maximum number of cells.

3.3 Results

3.3.1 Doxorubicin in MCF-7 Cells

Our method produced IC_{50} estimates similar to estimates derived using current techniques. Figure 3.1 shows the predicted growth curves for MCF-7 cells treated with 0 nM, 200 nM, 500 nM, and 1000 nM of doxorubicin when it is assumed that doxorubicin reduces the growth rate (55). Our calculations show that the $\varepsilon_{\max}$ for doxorubicin in

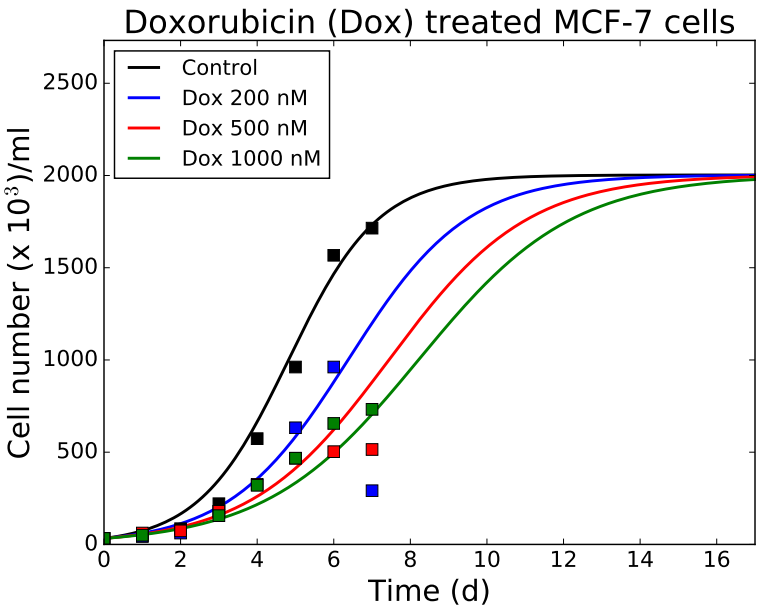

a	b	$\varepsilon_{\max}$	IC_{50}
0.853 mL/s	2000 cell/mL	0.500	210 nM

		SSR	$\varepsilon_{\max}$	IC_{50}
Confidence	25th	1.11	0.668	206.38 nM
Intervals	95th	3.96	31.05	42547.55 nM

Figure 3.1: We assume that the drug reduces the growth rate, which is parameter a. The growth of MCF-7 cells treated with 0 nM, 200 nM, 500 nM, and 1000 nM of doxorubicin is shown for data from (55). The 95% confidence interval is shown in the second table for the data sets. Values were sorted using Excel. Then the 25th and the 975th values were selected from the data.

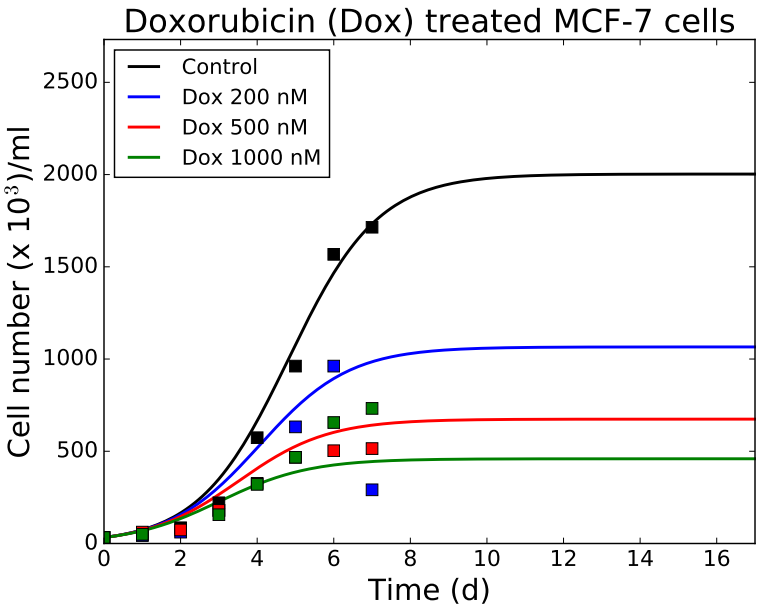

a	b	ε_{max}	IC_{50}
0.853 mL/s	2000 cell/mL	0.919	193 nM

		SSR	ε_{max}	IC_{50}
Confidence	25th	9.35	1.00	0.454 nM
Intervals	95th	27.6	2.98×10^{9}	2.98×10^{11} nM

Figure 3.2: We assumed that doxorubicin reduces the maximum number of MCF-7 cells.The data is from (55) for 0 nM, 200 nM, 500 nM, and 1000 nM of doxorubicin in MCF-7 cells. The 95% confidence interval is shown in the second table for the data sets. The 25th and the 975th values were selected from the data after being sorted in Excel.

MCF-7 cells under the assumption of reduced growth rate is 0.500, and the IC_{50} is 210 nM. This means that 25% of the cells would die if a breast cancer patient was given 210 nM of doxorubicin.

Figure 3.2 shows the model predictions for cell growth for data from (55) when assuming that doxorubicin reduces the maximum number of cells. Under the assumption that doxorubicin reduces the maximum number of cells, we found an $\varepsilon_{\max}$ of 92% and an IC_{50} of 190 nM. Meaning that when a patient with this tumor growth is being treated they would need to be given 193 nM to kill 46% of the cancer cells.

Estimated error was completed using the percentile bootstrap method for parameter a and parameter b. Fit residuals were sampled with replacement to create 1,000 bootstrap replicates of the data sets. Then a 95% confidence interval was estimated using these data sets. A 95% confidence interval means that after putting the data set in numerical order and we want to look at the 25th and the 975th values. The values were sorted using the sort function in Excel. The confidence interval values can be found in the second table in Figure 3.1 for the growth rate and the second table in Figure 3.2 for the carrying capacity. The $\varepsilon_{\max}$ values should be less than 1, so it is a problem that the values are approximately 31 times larger than they are supposed to be.

Our estimated of values for drug efficacy of doxorubicin in MCF-7 cells will not necessarily be the exact measurement that will be found for previous experiments. Recent experimental estimates for IC_{50} are in the range of 100-6000 nM which is similar to our estimates are 193 nM and 210 nM (56, 57, 58, 59, 60).

3.4 Summary

We developed and tested a method for estimating the drug efficacy parameters, IC_{50} and $\varepsilon_{\max}$, through the use of tumor growth data. We used this data to find time-independent parameters. To find these values we fit the data to a logistic model using a truncated Newton algorithm. Our estimates were similar to current estimates that have been found using current techniques.

We used mathematical models to extract measurement time independent estimates of $\varepsilon_{\max}$ and IC_{50}. We determined values for $\varepsilon_{\max}$ and IC_{50} assuming doxorubicin reduces growth rate or reduces the maximum number of cells. The IC_{50} was similar in both cases, but doxorubicin is better at reducing the maximum number of cells. When assuming doxorubicin reduces the growth rate for MCF-7 cells we found an $\varepsilon_{\max}$ of 0.500 and an IC_{50} of 210 nM. If we assume that the drug reduces the maximum number of cells then we determined that the $\varepsilon_{\max}$ is 0.92 and the IC_{50} is 190 nM.

Chapter 4

Discussion/Conclusions

4.1 Questions Answered

1. How does model choice affect the predicted IC_{50} and ε_{max}?

This paper examined several commonly used ODE models of tumor growth and quantitatively assesses the differences in their predictions of clinically relevant quantities. The models used were the exponential, Mendelsohn, logistic, linear, surface, Bertalanffy, and Gompertz model. We used experimental tumor growth data along with these equations to compare predicted values. We found that none of the models give the correct IC_{50} and ε_{max} values because they do not give the value of 1. An exception is the ε_{max} values when drugs reduce parameters b and c for the Gompertz model. While the exact amount of variation in predictions between different models will differ for other data sets, we expect that there will be disagreement in model predictions for all data sets.

2. Can a better way to measure IC_{50} and ε_{max} be found using mathematical modeling?

The method we used results in a single IC_{50} and ε_{max} for the entire data set. This is important because having a single result for the entire data set means that IC_{50} and ε_{max} do not depend on the day that the measurement is taken. The IC_{50} and ε_{max} values characterize how growth rate or carrying capacity are affected by a drug rather than how tumor volume on a particular day is affected by the drug. We found that our estimates for IC_{50} are within the range of current estimates.

4.2 Discussion

4.2.1 Extracting Drug Efficacy Parameters with Model Fitting

These findings suggest that modelers and clinicians must carefully consider their choice of growth model and how different growth assumptions might alter model predictions of the efficacy of treatment.

While our findings could be dismissed because the models and the implementation of chemotherapy are highly simplified, we believe they highlight a significant problem. While many mathematical models used for clinical assessment of patients and development of radiation or chemotherapy plans are more complex than those presented here (61), they must all make some assumption of how the tumor will grow. Due to the complexity of these models, however, it is difficult to trace the effect of the choice of growth model and determine how this choice might alter the model‘s predictions. In fact, while model

predictions are often assessed for sensitivity to errors in estimates of the parameters (62, 63), the effect of model assumptions is often neglected. Our findings, however, indicate that these assumptions could have a profound effect on model predictions since our simple models show that different choices of growth model result in large variations in model predictions. The results of these inaccuracies could have significant impacts on patient outcomes since we might either provide too much treatment, causing more severe side effects, or too little treatment, possibly resulting in continued growth of the tumor.

While some research has attempted to find the best ODE model to describe tumor growth (38, 39, 40, 41), the results seem to suggest that there are no broad guidelines; the most appropriate model seems to be dependent on the details of the experiment.

4.2.2 Modeling of Drug Treatment Assays

Our results found IC_{50} and $\varepsilon_{\max}$ values represent the drug effect on the growth rate or the drug effect on carrying capacity rather than reduction in the number of cells on a particular day. We found that our estimated values for drug efficacy of doxorubicin in MCF-7 cells wasn't necessarily the exact same as measurements that were found for previous experiments. Recent experimental values for IC_{50} are between 100 nM and 6000 nM. This is similar to our estimates of 193 nM and 210 nM (56, 57, 58, 59, 60). But, 193 nM and 210 nM are on the lower end of previous experimental estimates, meaning that patients might be given too high of a dose leading to increased toxic side effects and it would be predicted that a low percentage of cells will be killed at this dose.

One of the largest problems that we have with data sets is that measurements are not taken for long periods of time, like the data set we used from (55).

4.3 Implications for Work

We want a time independent IC_{50} because if IC_{50} depends on measurement day then the amount of drug a patient is recommended will depend on what day IC_{50} is measured. It is important to make sure the patient gets the right amount of drugs. Chemotherapy drugs are toxic to both cancerous and non-cancerous cells which is one reason why you do not want to give a patient the wrong dose of drugs. There are a lot of side effects from chemotherapy due to cancerous and non-cancerous cells being killed. One of the more dangerous side effects for doxorubicin is cardiotoxicity (64). Another reason why a patient shouldn't be given an incorrect amount of chemotherapy drugs is because the drugs are supposed to stop the growth and stop the cells from migrating throughout the body. If a patient is not given enough drugs, then the tumor will continue to grow and the patient will not get better. If too high of a dose is given to a patient then it will be toxic and kill too many non-cancerous cells. Killing too many non-cancerous cells can lead to a patient having a weak immune system and become susceptible to infections (64).

If the day picked to make the IC_{50} and $\varepsilon_{\max}$ measurements is too early, then the $\varepsilon_{\max}$ value that is estimated will be too small and the IC_{50} value will be too large. The general trend found for all models is that the measured IC_{50} value decreases with increasing measurement day. The only exceptions to this trend are the logistic and the

Bertalanffy model when it is assumed that the drug effects parameter b. This means that if the measurement day that is chosen to determine the dose of drugs that the patient is getting is too early, then the patient will be given too much drugs.

4.4 Conclusions

It is our hope that the findings presented here will spur more investigation into the effect of choice of cancer growth model on predicted treatment outcomes and that researchers will consider more than just best fit when selecting a growth model. Our hope is to be able to complete our procedure on longer data sets and to use what we learned about time independent drug efficacy parameters in order to not have a time-dependence bias.

4.5 Future Work

4.5.1 Test Parameter Estimation Technique with Known Anticancer Agents

We will first optimize our parameter estimation technique to return the correct values of IC_{50} and ε_{max}. This will be done by applying our method to extract IC_{50} and ε_{max} of common anticancer drugs, doxorubicin, paclitaxel and gemcitabine, and comparing our results to previous published studies. Three cell lines (HEK-293, HeLa and MCF-7) will be cultured and the cell population will be assessed via a cell counter.Collecting our own data allows us to standardize the initial conditions for all cell lines being used to optimize our parameter estimation technique when determining the correct IC_{50} and ε_{max} values.

It also allows us to test our estimation technique on longer data sets because we are able to control the length of the data set. We will collect cell population data daily for the period of 2 weeks, measuring both active and necrotic cells, to obtain a sufficient number of data points for modeling.

In our experiments, non-cancerous HEK-293 cells will serve as a control for the growth of cancerous HeLa and MCF-7 cells. Broadly, this goal requires that we find an appropriate growth model to describe growth of cancer cells in culture. We then need to determine the best model for drug treatment with each test drug. Finally, we will put the growth model together with the model of the drug effect to extract the IC_{50} and $\varepsilon_{\max}$ similar to the methods that are used in chapter 3.

This work can be used to develop better treatment plans for patient's receiving cancer treatments in hospitals. This test parameter estimation technique is vital because it is important that a patient isn't given an incorrect drug dose. Time independent IC_{50} values are needed because without them a patient's treatment can ineffective.

4.5.2 Calculate Shape of Systematic Analysis Curve

We will use this equation

$$1 - \frac{V_{\text{drug}}}{V_{\text{no drug}}} = 1 - \frac{V_0 e^{(1-\epsilon)aT_m}}{V_0 e^{aT_m}} \tag{4.1}$$

where V_{drug} is the number of cells after drugs are applied to the cells, $V_{\text{no drug}}$ is the number of cells when no drugs are applied to cells, ϵ is the drug efficiency, V_0 is the initial

number of cells, a is the growth rate, and T_m is the measurement time. This equation is for the exponential model because it will be the easiest model to solve for.

Our hope is to be able to find the shape of the curve because then we will be able to find the values for $\varepsilon_{\max}$ and IC_{50} values for each of the curves. To do this we would need to get rid of the exponentials and be able to rearrange the right side of the equation to look like the form of the drug efficiency equation.

4.5.3 Test Model Fitting on Theoretical Data

To test model fitting on theoretical data we would generate a data set and then see if we can get the correct predicted fit. To do this we would add gaussian noise to the data points with a mean of zero and a standard deviation of 10 percent. The data points will be created from the logistic model. The data will then be fit to the seven ODE models to see the effect of noise on the fit. We want to know what would happen to the fit if the data is fit with another model and if the best fit is still the logistic model after noise is added to the data points.

Appendix A

Additional Graphs

A.1 Graphs for Experimental Research

The graphs model tumor growth for HeLa (cervical cancer cells), HEK-293 (human embryonic kidney cells), and MCF-7 (breast cancer cells) cells using the seven differential equations. In low-income and middle-income countries breast cancer and cervical cancer result in more morbidity and mortality than in high-income patients. This has resulted in breast cancer and cervical cancer being major global health problems (10).

Cervical cancer is an important global issue to study because it is the third most commonly diagnosed cancer for women throughout the world. When cervical cancer is in the early stages there is a 91 % survival, while the chance of survival decreases to 57 percent after the disease has spread locally and 16 percent when it spreads throughout the body (54).

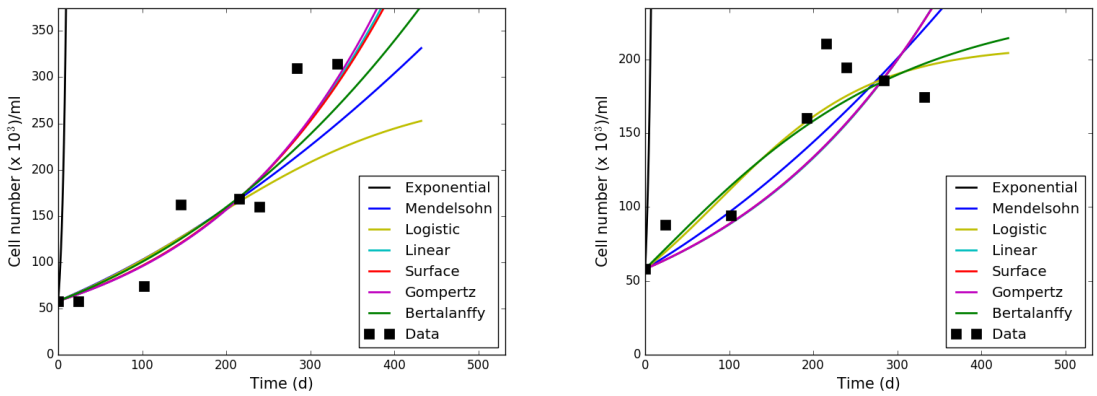

Figure A.1: This graph models tumor growth for HeLa cells.

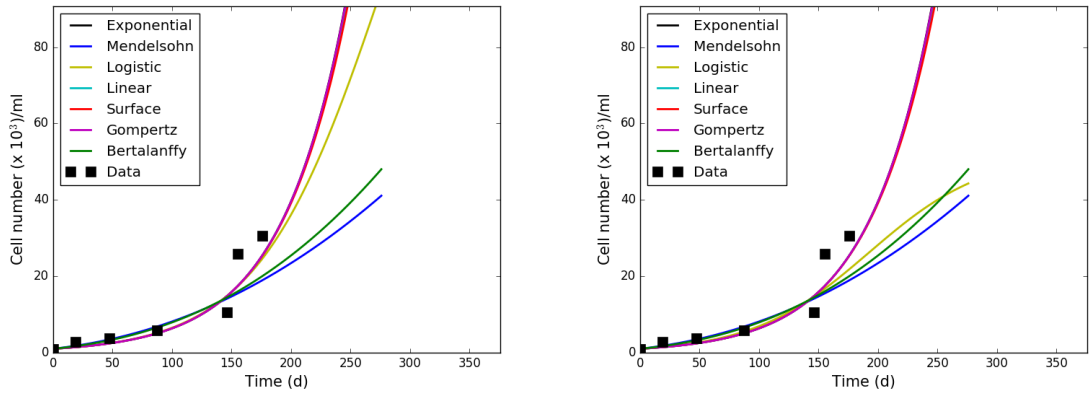

Figure A.2: This graph models tumor growth for HEK-293 cells.

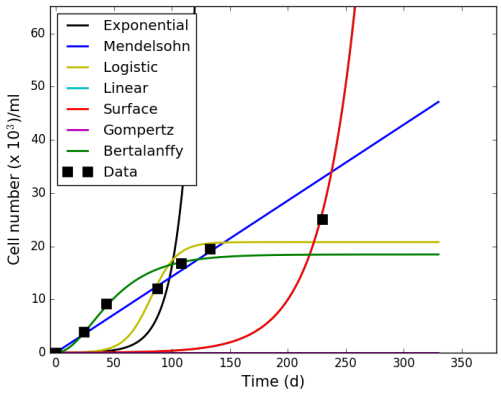

Figure A.3: This graph models tumor growth for MCF-7 cells.

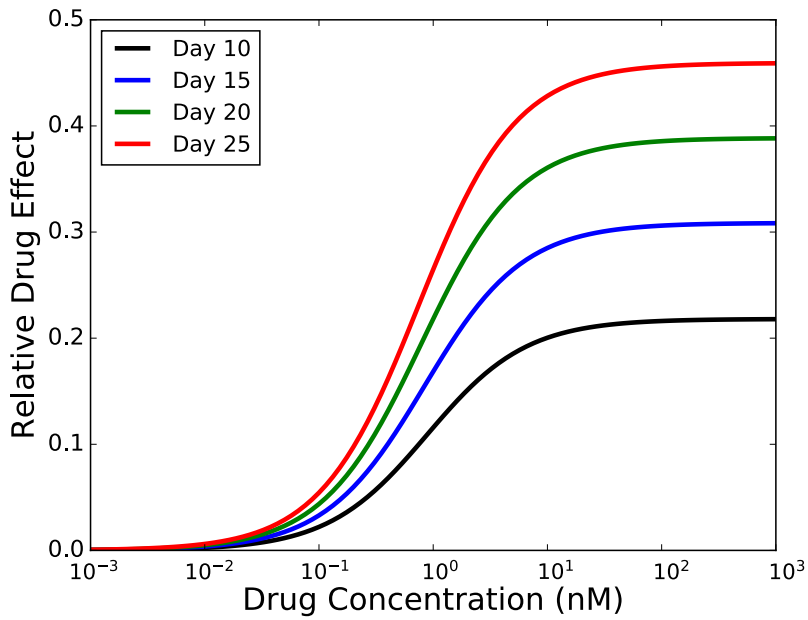

Days	$\varepsilon_{\max}$	IC_{50}
Day 10	0.255	0.885
Day 15	0.357	0.832
Day 20	0.445	0.784
Day 25	0.521	0.738

Figure A.4: Exponential Model, Reduce a. $\varepsilon_{\max}$ and IC_{50} estimates are given in the table below the graph.

A.2 Exponential Model

It can be seen in Figure A.4 that $\varepsilon_{\max}$ increases with increasing measurement time, while IC_{50} decreases with increasing measurement day when the drug effect is applied to a. The table included in Figure A.4 shows when $\varepsilon_{\max}$ and IC_{50} are calculated for drugs having an effect on a.

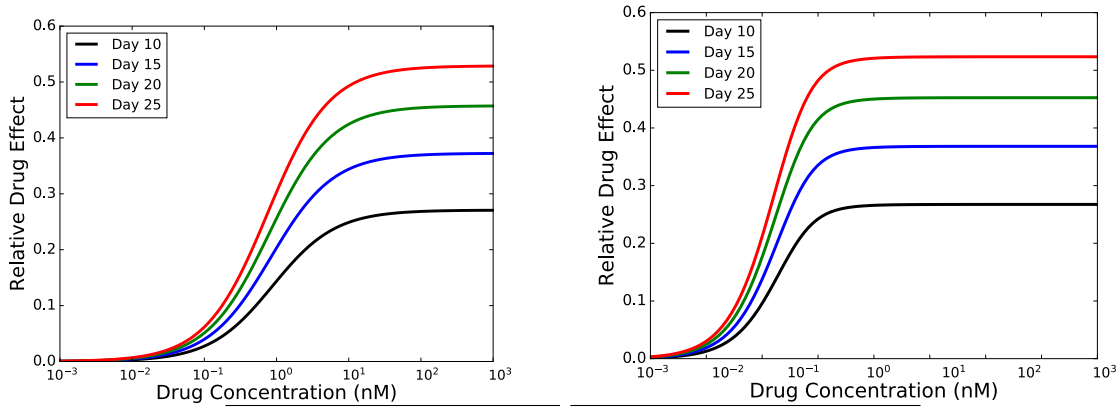

Days	$\varepsilon_{\max}$	IC_{50}
Day 10	0.271	0.884
Day 15	0.372	0.834
Day 20	0.457	0.789
Day 25	0.529	0.749

Days	$\varepsilon_{\max}$	IC_{50}
Day 10	0.267	0.0471
Day 15	0.368	0.045
Day 20	0.453	0.043
Day 25	0.523	0.041

Figure A.5: Mendelsohn model, reduce a (left) and reduce b (right). $\varepsilon_{\max}$ and IC_{50} estimates are given in the tables below the graph.

A.3 Mendelsohn Model

Both graphs in Figure A.5 show that $\varepsilon_{\max}$ increases with increasing measurement time, while IC_{50} decreases with increasing measurement day. The table on the left included in Figure A.5 shows when $\varepsilon_{\max}$ and IC_{50} are calculated for drugs having an effect on a and the table on the right shows when $\varepsilon_{\max}$ and IC_{50} are calculated for drugs having an effect on b.

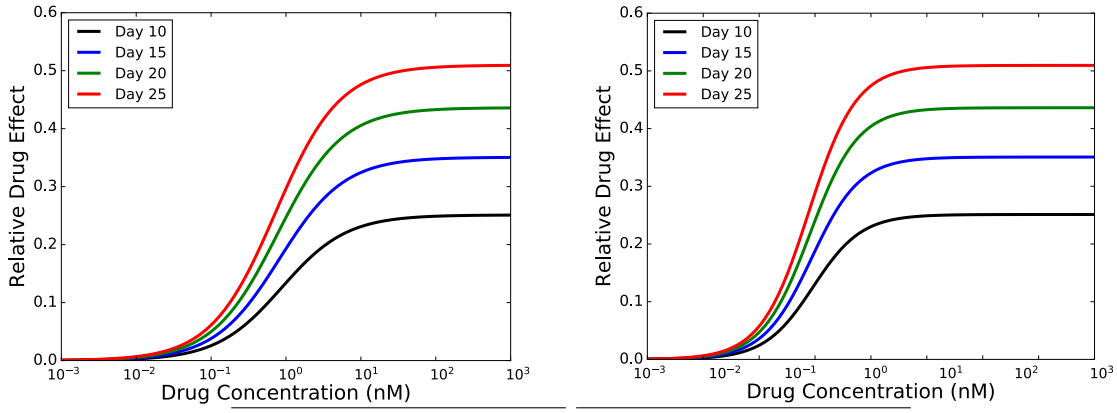

Days	$\varepsilon_{\max}$	IC_{50}
Day 10	0.251	0.873
Day 15	0.350	0.818
Day 20	0.436	0.768
Day 25	0.509	0.723

Days	$\varepsilon_{\max}$	IC_{50}
Day 10	0.251	0.176
Day 15	0.351	0.168
Day 20	0.436	0.160
Day 25	0.510	0.153

Figure A.6: Linear model, reduce a (left) and reduce b (right). $\varepsilon_{\max}$ and IC_{50} estimates are given in the tables below the graph.

A.4 Linear Model

In Figure A.6 it can be seen that both graphs show that $\varepsilon_{\max}$ increases with increasing measurement time, while IC_{50} decreases with increasing measurement day. For both graphs $\varepsilon_{\max}$ is almost identical, but IC_{50} is very different for each of the graphs. The table on the left included in Figure A.6 shows when $\varepsilon_{\max}$ and IC_{50} are calculated for drugs having an effect on a and the table on the right shows when $\varepsilon_{\max}$ and IC_{50} are calculated for drugs having an effect on b.

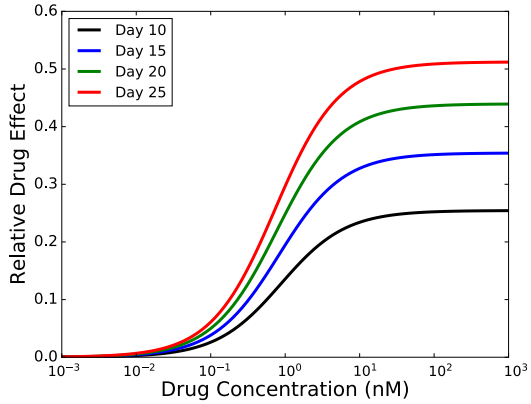

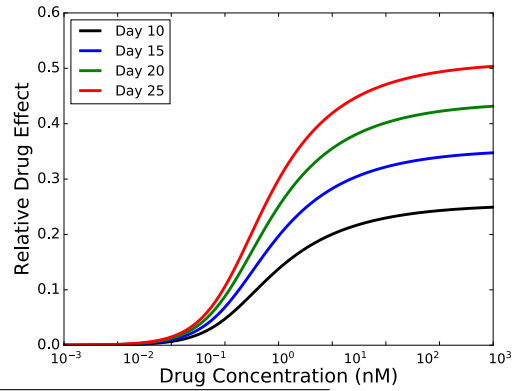

Days	$\varepsilon_{\max}$	IC_{50}
Day 10	0.254	0.876
Day 15	0.354	0.822
Day 20	0.439	0.773
Day 25	0.512	0.730

Days	$\varepsilon_{\max}$	IC_{50}
Day 10	0.255	0.774
Day 15	0.357	0.731
Day 20	0.445	0.694
Day 25	0.521	0.661

Figure A.7: Surface model, reduce a (left) and reduce b (right). $\varepsilon_{\max}$ and IC_{50} estimates are given in the tables below the graph.

A.5 Surface Model

Both graphs in Figure A.7 show that $\varepsilon_{\max}$ increases with increasing measurement time, while IC_{50} decreases with increasing measurement day. $\varepsilon_{\max}$ and IC_{50} are similar for both of the graphs even though the shape of the lines are different in each of the graphs. The table on the left included in Figure A.7 shows when $\varepsilon_{\max}$ and IC_{50} are calculated for drugs having an effect on a and the table on the right shows when $\varepsilon_{\max}$ and IC_{50} are calculated for drugs having an effect on b.

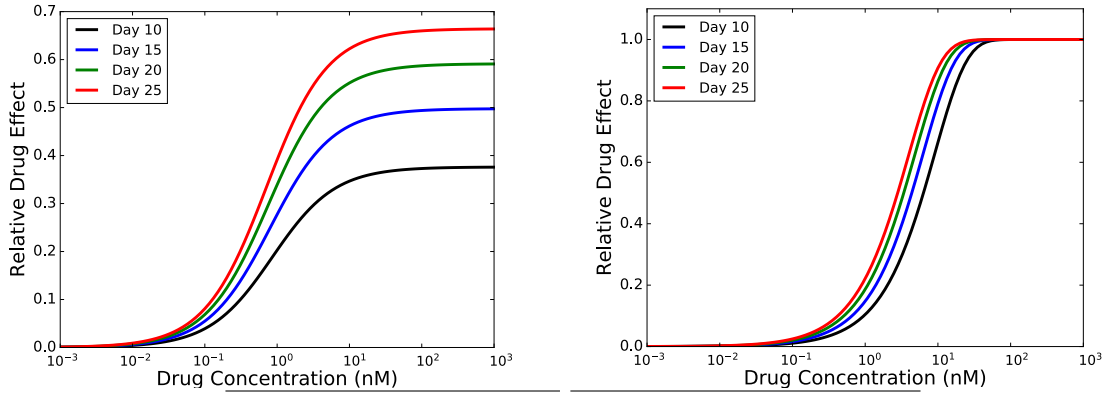

Days	$\varepsilon_{\max}$	IC_{50}
Day 10	0.376	0.856
Day 15	0.497	0.798
Day 20	0.591	0.748
Day 25	0.664	0.705

Days	$\varepsilon_{\max}$	IC_{50}
Day 10	1.0595	6.579
Day 15	1.053	4.977
Day 20	1.049	3.765
Day 25	1.046	2.848

Figure A.8: Bertalanffy model, reduce a (left) and reduce b (right). $\varepsilon_{\max}$ and IC_{50} estimates are given in the table below the graph.

A.6 Bertalanffy Model

The table on the left included in Figure A.8 shows when $\varepsilon_{\max}$ and IC_{50} are calculated for drugs having an effect on a and the table on the right shows when $\varepsilon_{\max}$ and IC_{50} are calculated for drugs having an effect on b. The largest difference between the relative drug effect on a and the relative drug effect on b is that $\varepsilon_{\max}$ increases with measurement time for Figure A.8 (left) but $\varepsilon_{\max}$ stays constant with measurement time for Figure A.8 (right). In can also be seen from Figure A.8 IC_{50} decreases with measurement time for both graphs.

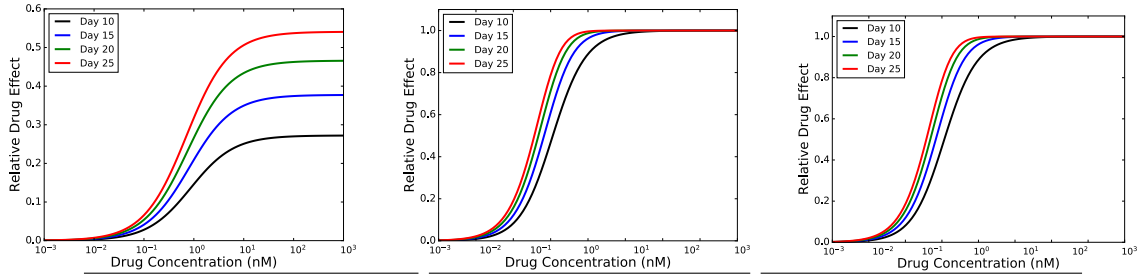

Days	$\varepsilon_{\max}$	IC_{50}
Day 10	0.272	0.863
Day 15	0.377	0.805
Day 20	0.466	0.754
Day 25	0.540	0.708

Days	$\varepsilon_{\max}$	IC_{50}
Day 10	1.00	0.207
Day 15	1.00	0.135
Day 20	1.00	0.102
Day 25	1.00	0.084

Days	$\varepsilon_{\max}$	IC_{50}
Day 10	1.00	0.210
Day 15	1.00	0.137
Day 20	1.00	0.104
Day 25	1.00	0.085

Figure A.9: Gompertz model, reduce a (left), reduce b (middle), and reduce c (right). $\varepsilon_{\max}$ and IC_{50} estimates are given in the table below the graph.

A.7 Gompertz Model

In the left graph in Figure A.9 it can be seen that $\varepsilon_{\max}$ increases with increasing measurement time, while IC_{50} decreases with increasing measurement day when the drug effect is applied to a. It can be seen from FigureA.9 (middle and right) that the drug effect is identical when applied to b and c. For both of these graphs (middle and right) IC_{50} decreases with time but $\varepsilon_{\max}$ stays constant with measurement time. The table on the left included in Figure A.9 shows when $\varepsilon_{\max}$ and IC_{50} are calculated for drugs having an effect on a, the table in the middle shows when $\varepsilon_{\max}$ and IC_{50} are calculated for drugs having an effect on b and the table on the right shows when $\varepsilon_{\max}$ and IC_{50} are calculated for drugs having an effect on c.

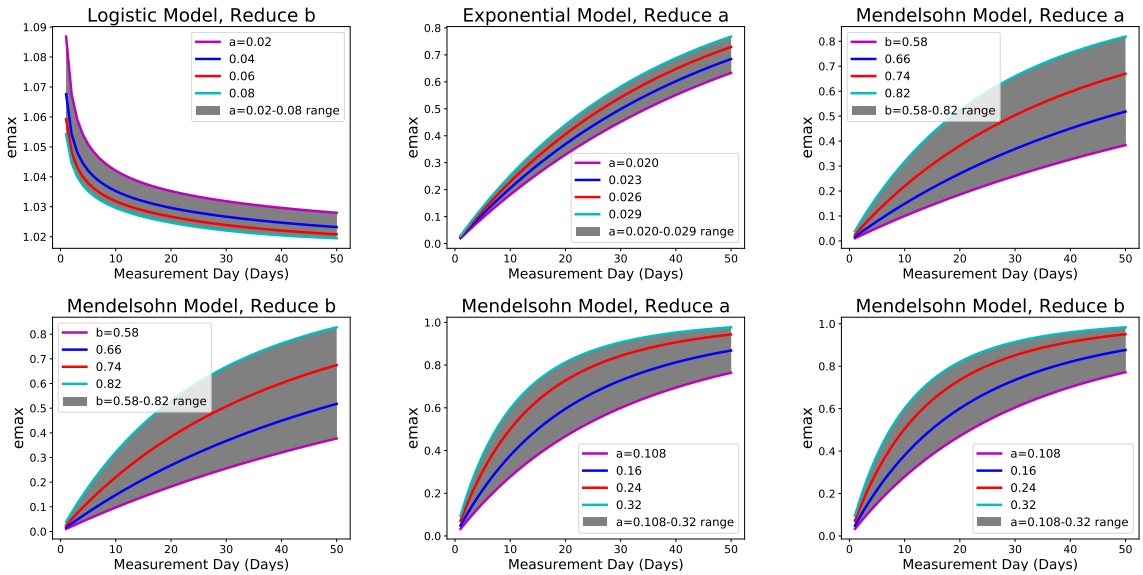

Figure A.10: $\varepsilon_{\max}$ graphs for systematic analysis, where parameters a, b, or c are varied.

A.8 $\varepsilon_{\max}$ and IC_{50} Graphs for the Sensitivity Analysis

In order to assess how our results depend on model parameters, we completed a sensitivity analysis by varying model parameters and re-running the simulations. Figures A.10, A.11, A.12, and A.13 are the remaining graphs for the sensitivity analysis that is completed in Ch 2.

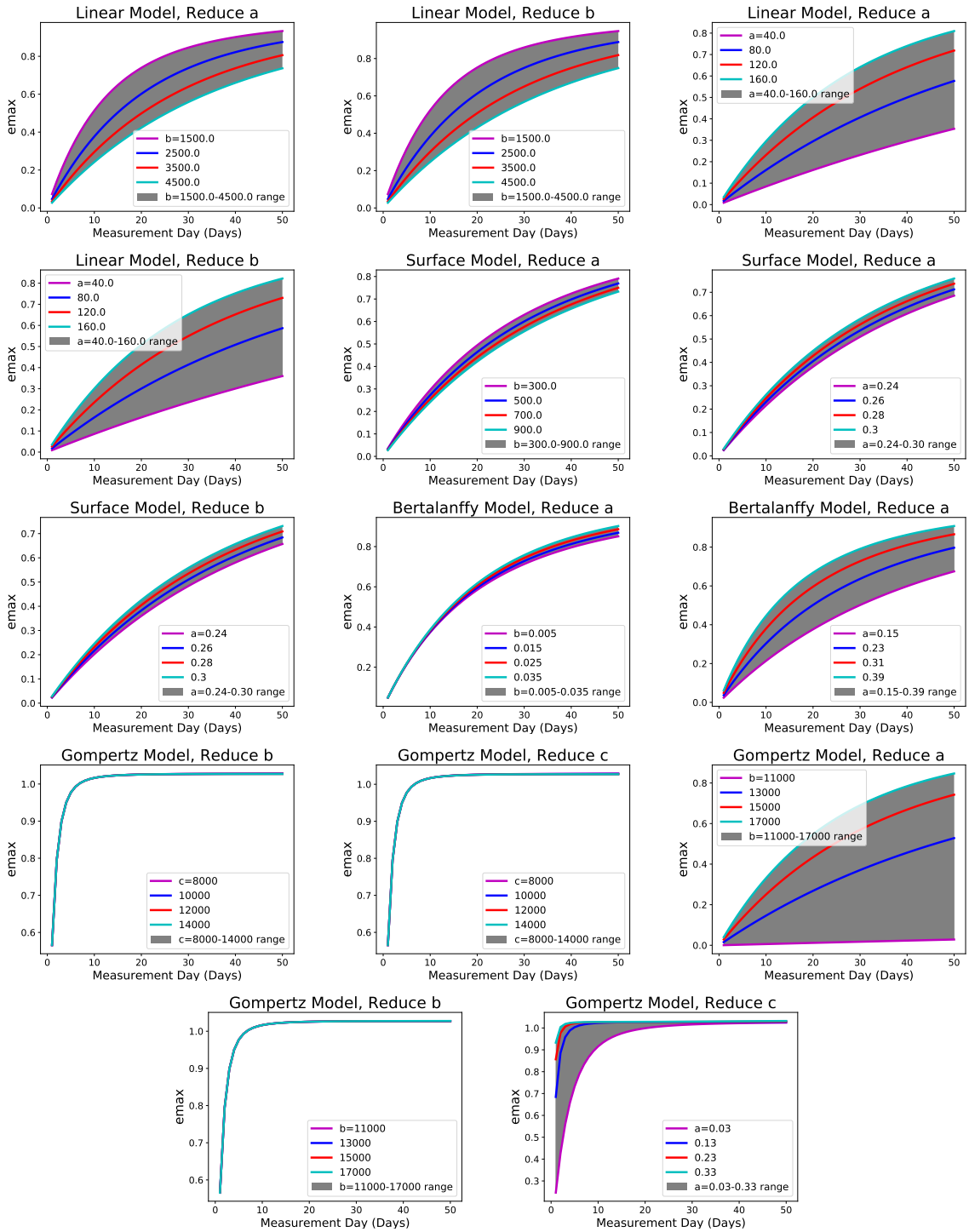

Figure A.11: $\varepsilon_{\max}$ graphs for systematic analysis, where parameters a, b, or c are varied.

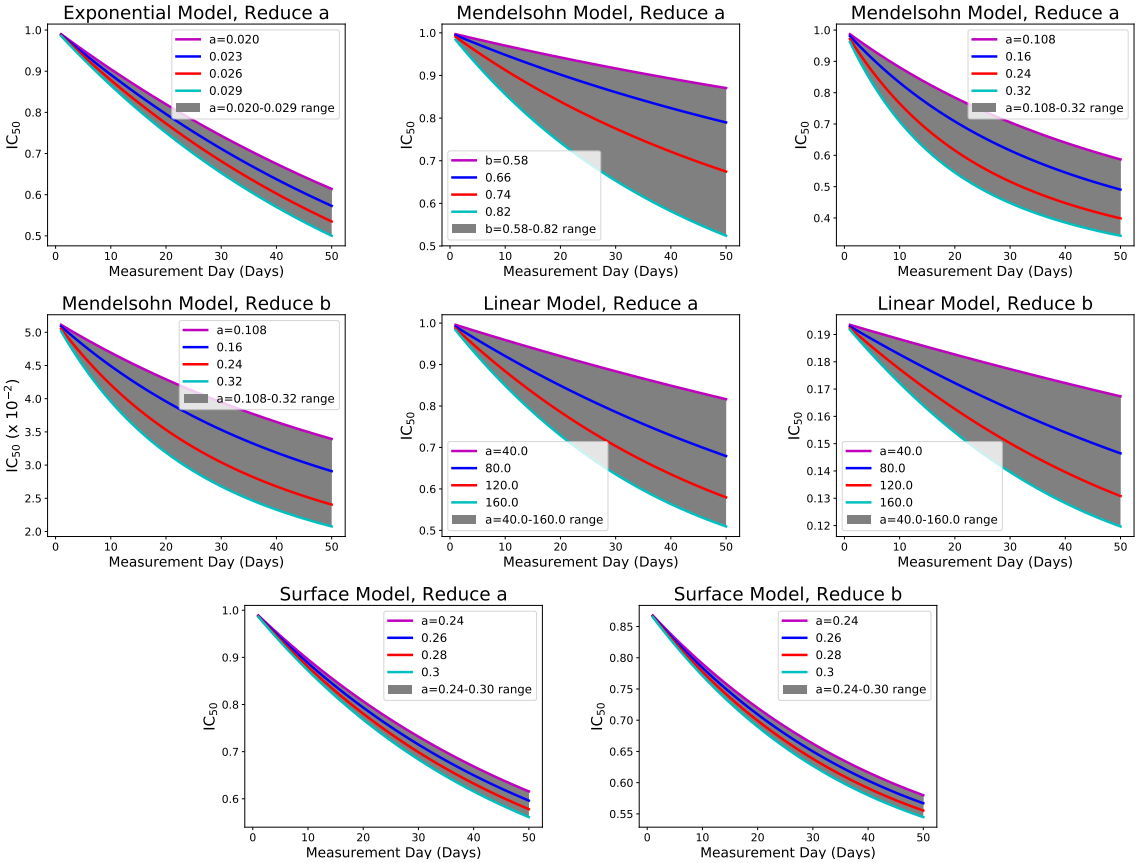

Figure A.12: IC_{50} graphs for systematic analysis, where parameters a, b, or c are varied.

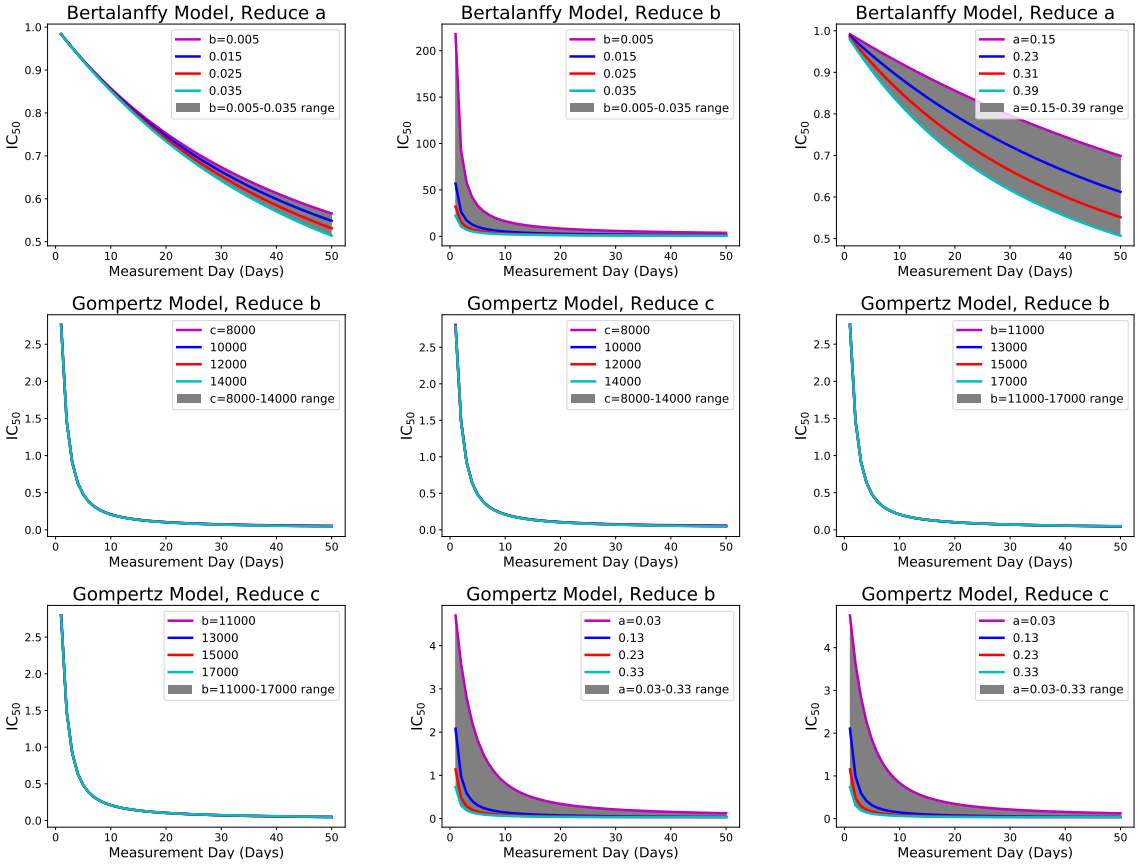

Figure A.13: IC_{50} graphs for systematic analysis, where parameters a, b, or c are varied.

Bibliography

[1] Paul Hanly, Alison Pearce, and Linda Sharp. The cost of premature cancer-related mortality: a review and assessment of the evidence. *Exp. Rev. Pharmacoecon. Outcomes. Res.*, 14(3):355–377, June 2014.

[2] Kathryn H. Schmitz, Tracey DiSipio, Louisa G. Gordon, and Sandra C. Hayes. Adverse breast cancer treatment effects: the economic case for making rehabilitative programs standard of care. *Supportive Care in Cancer*, 23(6):1807–1817, June 2015.

[3] Alan Carlotto, Virginia L. Hogsett, Elyse M. Maiorini, Janet G. Razulis, and Stephen T. Sonis. The economic burden of toxicities associated with cancer treatment: Review of the literature and analysis of nausea and vomiting, diarrhoea, oral mucositis and fatigue. *Pharmacoecon.*, 31(9):753–766, September 2013.

[4] Ronan Glynn, Ji Z. Chin, Michael J. Kerin, and Karl J. Sweeney. Representation of cancer in the medical literature - a bibliometric analysis. *PLOS One*, 5(11):e13902, November 9 2010.

[5] Anish Babu, Amanda K. Templeton, Anuparma Munshi, and Rajagopal Ramesh. Nanodrug delivery systems: A promising technology for detection, diagnosis, and treatment of cancer. *AAPS Pharmscitech*, 15(3):709–721, June 2014.

[6] Jonathan Pol, Norma Bloy, Florine Obrist, Alexander Eggermont, Jerome Galon, Isabelle Cremer, Philippe Erbs, Jean-Marc Limacher, Xavier Preville, and Laurence Zitvogel. Trial watch oncolytic viruses for cancer therapy. *Oncoimmunology*, 3:e28694, June 2014.

[7] C. Ceresa, A. Bravin, G. Cavaletti, M. Pellei, and C. Santini. The combined therapeutical effect of metal-based drugs and radiation therapy: The present status of research. *Curr. Med. Chem.*, 21(20):2237–2265, 2014.

[8] Babak Bakhshinejad, Marzieh Karimi, and Majid Sadeghizadeh. Bacteriophages and medical oncology: targeted gene therapy of cancer. *Med. Oncol.*, 31(8):110, August 2014.

[9] Masahide Kuroki and Naoto Shirasu. Novel treatment strategies for cancer and their tumor-targeting approaches using antibodies against tumor-associated antigens. *Anticancer Res*, 34(8):4481–4488, August 2014.

[10] Margaret M. Demment, Karen Peters, J. Andrew Dykens, Ann Dozier, Haq Nawaz, Scott McIntosh, Angela Sy Jennifer S. Smith6, Tracy Irwin, Thomas T. Fogg, Mahmooda Khaliq, Rachel Blumenfeld, Mehran Massoudi, and Timothy De Ver Dye. Developing the evidence base to inform best practice: A scoping study of breast and cervical cancer reviews in low- and middle- income countries. *PLoS ONE*, 10(9), September 2015.

[11] Zvia Agur and Stanimir Vuk-Pavlovic. Mathematical modeling in immunotherapy of cancer: Personalizing clinical trials. *Mol. Ther.*, 20(1):1–2, January 2012.

[12] Zvia Agur, Moran Elishmereni, and Yuri Kheifetz. Personalizing oncology treatments by predicting drug efficacy, side-effects, and improved therapy: mathematics, statistics, and their integration. *Wiley Interdiscip. Rev. Syst. Biol. Med.*, 6(3):239–253, May 2014.

[13] G.-M. Hu, C.-Y. Lee, Y.-Y. Chen, N.-N. Pang, and W. J. Tzeng. Mathematical model of heterogeneous cancer growth with an autocrine signaling pathway. *Cell Prolif.*, 45(5):445–455, October 2012.

[14] Drew Pardoll. Does the immune system see tumors as foreign or self? *Annu. Rev. Immunol.*, 21:807–839, April 2003.

[15] Lynn C. Hartmann and Charles L. Loprinzi. *The Mayo Clinic Breast Cancer Book*. Good Books, P.O. Box 419, Intercourse, PA 17534, 1st edition, 2012.

[16] Alberto d'Onofrio. Tumor evasion from immune control: Strategies of a miss to become a mass. *Chaos Soliton Fract*, 31(2):261–268, January 2007.

[17] Sifeng Mao Shuo Feng Weiwei Li, Mashooq Khan and Jin-Ming Lin. Advances in tumor-endothelial cells co-culture and interaction on microfluidics. *Journal of Pharmaceutical Analysis*, 8(4):210–218, August 2018.

[18] G. De Nicolao I. Poggesi A. Marsiglio D. Ballinari M. Germani, P. Magni and M. Rocchetti. In vitro cell growth pharmacodynamic studies: a new nonparametric approach to determining the relative importance of drug concentration and treatment time. *Cancer Chemotherapy Pharmacology*, 52(6):507–513, December 2003.

[19] Shawn P. Garbett KeishacN. Hardeman B. Bishal Paudel Carlos F. Lopez Vito Quaranta Leonard A. Harris, Peter L. Frick and Darren R. Tyson. An unbiased metric of antiproliferative drug effect in vitro. *Nature Methods*, 13(6), June 2016.

[20] Jan Elias, Luna Dimitrio, Jean Clairambault, and Roberto Natalini. The p53 protein and its molecular network: Modelling a missing link between dna damage and cell fate. *Biochim. Biophys. Acta, Proteins Proteomics*, 1844(1):232–247, January 2014.

[21] Anna Kane Laird. Dynamics of tumor growth. *Br. J. Cancer*, 19(2):278–291, 1965.

[22] Anna Kane Laird. Dynamics of tumor growth. *Br. J. Cancer*, 13:490–502, 1964.

[23] WC Summers. Dynamics of tumor growth — a mathematical model. *Growth*, 30(3):333, 1966.

[24] Lyle A. Dethlefsen, J.M.S. Prewitt, and M.L. Mendelsohn. Analysis of tumor growth curves. *J. Nat. Cancer Inst.*, 40(2):389–405, 1968.

[25] N. Patrik Brodin, Ivan R. Vogelius, Thomas Bjork-Eriksson, Per Munck af Rosenschold, Maja V. Maraldo, Marianne C. Aznar, Lena Specht, and Soren M. Bentzen. Optimizing the radiation therapy dose prescription for pediatric medulloblastoma: Minimizing the life years lost attributable to failure to control the disease and late complication risk. *Acta Oncologica*, 53(4):462–470, April 2014.

[26] Yazdan Batmani and Hamid Khaloozadeh. Optimal drug regimens in cancer chemotherapy: A multi-objective approach. *Comput. Biol. Med.*, 43:20892095, 2013.

[27] Xuelin Huang, Jing Ning, and Abdus S. Wahed. Optimization of individualized dynamic treatment regimes for recurrent diseases. *Stat. Med.*, 33(14):2363–2378, June 2014.

[28] Erica E.M. Moodie, Thomas S. Richardson, and David A. Stephens. Demystifying optimal dynamic treatment regimes. *Biom.*, 63(2):447–455, June 2014.

[29] Zhihui Wang and Thomas S. Deisboeck. Mathematical modeling in cancer drug discovery. *Drug Discovery Today*, 19(2):145–150, February 2014.

[30] John Carl Panetta. A mathematical model of drug resistance: Heterogeneous tumors. *Math Biosci*, 147:41–61, 1998.

[31] C. M. Sakode, R. Padhi, S. Kapoor, V.P.S. Rallabandi, and P.K. Roy. Multimodal therapy for complete regression of malignant melanoma using constrained nonlinear optimal dynamic inversion. *Biomed. Signal Process. Control*, 13:198–211, September 2014.

[32] L.G. de Pillis, W. Gu, and A.E. Radunskaya. Mixed immunotherapy and chemotherapy of tumors: modeling, applications and biological interpretations. *J. Theo.Biol.*, 238(4):841–862, 21 February 2006.

[33] J. C. Panetta. A logistic model of periodic chemotherapy with drug resistance. *Appl. Math. Lett.*, 10(1):123–127, January 1997.

[34] Jasmine Foo and Franziska Michor. Evolution of acquired resistance to anti-cancer therapy. *J. Theor. Biol.*, 355:10–20, August 21 2014.

[35] Philip Gerlee. The model muddle: In search of tumor growth laws. *Cancer Res.*, 73(8):2407–11, February 2013.

[36] Dominik Wodarz and Natalia Komarova. Towards predictive computational models of oncolytic virus therapy: Basis for experimental validation and model selection. *PLoS One*, 4(1):1–12, January 2009.

[37] J. R. Usher. Some mathematical models for cancer chemotherapy. *Computers Math. Applic*, 28(9):73–80, 1994.

[38] Vinay G. Vaidya and Jr. Frank J. Alexandro. Evaluation of some mathematical models for tumor growth. *Int. J. Bio-Med. Comput.*, 13(1):19–35, January 1982.

[39] E.A. Sarapata and L.G. de Pillis. A comparison and catalog of intrinsic tumor growth models. *Bull. Math. Biol.*, 76(8):2010–2024, 1 August 2014.

[40] Sebastien Benzekry, Clare Lamont, Afshin Beheshti, Amanda Tracz, John M.L. Ebos, Lynn Hlatky, and Philip Hahnfeldt. Classical mathematical models for description and prediction of experimental tumor growth. *Plos Comp. Biol.*, 10(8):e1003800, August 2014.

[41] Niklas Hartung, Séverine Mollard, Dominique Barbolosi, Assia Benabdallah, Guillemette Chapuisat, Gerard Henry, Sarah Giacometti, Athanassios Iliadis, Joseph Ciccolini, Christian Faivre, and Florence Hubert. Mathematical modeling of tumor growth and metastatic spreading: Validation in tumor-bearing mice. *Cancer Res.*, 74(22):6397–6407, 15 November 2014.

[42] V.P Collins, R.K. Loeffler, and H. Tivey. Observations on growth rates of human tumors. *Am. J. Roentgenol. Radium Ther. Nuc. Med.*, 78(5):988–1000, 1956.

[43] Anne Talkington and Rick Durrett. Estimating tumor growth rates in vivo. *Bull Math Biol*, 77(10):1934–54, October 2015.

[44] M.L. Mendelsohn. Cell proliferation and tumor growth. In L.F. Lamberton and R.J.M. Fry, editors, *Cell Proliferation*, pages 190–210. Oxford-Blackwell Scientific Publication, 1963.

[45] Pierre-Francois Verhulst. Notice sur la loi que la population poursuit dans son accroissement. *Correspondance mathmatique et physique*, 10:113–121, 1838.

[46] H.M Patt and M.E. Blackford. Quantitative studies of the growth response of the Krebs ascites tumor. *Cancer Res.*, 14(5):391–396, 1954.

[47] L. von Bertalanffy. Problems of organic growth. *Nature*, 163(4135):156–158, 1949.

[48] Benjamin Gompertz. On the nature of the function expressive of the law of human mortality, and on a new method of determining the value of life contingencies. *Phil. Trans. Roy. Soc.*, 27:513–585, 1825.

[49] Charles P. Winsor. The gompertz curve as a growth curve. 18(1):1–8, 1932.

[50] Hana Jaafari Hope Murphy and Hana M Dobrovolny. Differences in predictions of ode models of tumor growth: A cautionary example. *BMC Cancer*, 16(1):163–173, 2016.

[51] Andrea Worschech, Nanhai Chen, Yong A Yu, Qian Zhang, Zoltan Pos, Stephanie Weibel, Viktoria Raab, Marianna Sabatino, Alessandro Monaco, Hui Liu, Vladia Monsurr, R Mark Buller, David F Stroncek, Ena Wang, Aladar A Szalay, and Francesco M Marincola. Systemic treatment of xenografts with vaccinia virus GLV-1h68 reveals the immunologic facet of oncolytic therapy. *BMC Genomics*, 10:301, 2009.

[52] M. G. Wientjes J. E. Kains, N. J. Millenbaugh and J. L.-S. Au. Design and analysis of in vitro antitumor pharmacodynamic studies. *Cancer Resolution*, 55(2), November 1995.

[53] Anita Sveen, Bjarne Johannessen, Manuel R Teixeira, Ragnhild A Lothe, and Rolf I Skotheim. Transcriptome instability as a molecular pan-cancer characteristic of carcinomas. *BMC Genom.*, 15(1):672, August 2014.

[54] Stanculeanu DL, Daniela Zob, Lazescu A, Bunghez R, and Anghel. Development of new immunotherapy treatments in different cancer types. *J Med Life*, 9(3):240–248, July 2016.

[55] Eva Slaba Kamila Lacjakova Marianna Trebunova, Galina Laputkova and Aneta Verebova. Effects of docetaxel, doxorubicin and cyclophosphamide on human breast cancer cell line mcf-7. *Anticancer Research*, 32(7):2849–2854, July 2012.

[56] M. Alagumuthu and S. Arumugam. Molecular explorations of substituted 2-(4-phenylquinolin-2-yl) phenols as phosphoinositide 3-kinase inhibitors and anticancer agents. *Cancer Chemotherapy Pharmacology*, 79(2):389–397, February 2017.

[57] M. M. Anwar H. I. Ali T. M. Abdel-Ghani K. M. Amin, Y. M. Syam and A. M. Serry. Synthesis and molecular docking studies of new furochromone derivatives as p38alpha mapk inhibitors targeting human breast cancer mcf-7 cells. *Cell Proliferation*, 25(8):2423–2436, April 2017.

[58] E. S. H. El Ashry A. T. Boraei, M. S. Gomaa and A. Duerkop. Design, selective alkylation and x-ray crystal structure determination of dihydro-indolyl-1,2,4-triazole- 3-thione and its 3-benzylsulfanyl analogue as potent anticancer agents. *Cancer Chemotherapy Pharmacology*, 125:360–371, January 2017.

[59] Viviane R. Sipowo Tala Jacob O. Midiwo Armelle T. Mbaveng-Sauda Swaleh Oğuzhan Karaosmanoğlu Victor Kuete, Leonidah K. Omosa and Hulya Sivas. Cytotoxicity of plumbagin, rapanone and 12 other naturally occurring quinones from kenyan flora towards human carcinoma cells. *BMC Pharmacology and Toxicology*, 17(60), December 2016.

[60] M. S. Salem and M. A. M. Ali. Novel pyrazolo[3,4-b]pyridine derivatives: Synthesis, characterization, antimicrobial and antiproliferative profile. *Biological and Pharmaceutical Bulletin*, 39(4).

[61] Loredana G. Marcu and Wendy M. Harriss-Phillips. In silico modelling of treatment-induced tumour cell kill: Developments and advances. *Comp. Math. Meth. Med.*, 2012:960256, 2012.

[62] Anna Hoffmann, Alexander Scherrer, and Karl-Heinz K ufer. Analyzing the quality robustness of chemotherapy plans with respect to model uncertainties. *Math. Biosci.*, 259:55–61, 29 November 2015.

[63] Michael Krause, Alexander Scherrer, and Christian Thieke. On the role of modeling parameters in IMRT plan optimization. *Phys. Med. Biol.*, 53(18):4907–4926, September 28 2008.

[64] Pornsak Sriamornsak Oktay Tacar and Crispin R. Dass. Doxorubicin: an update on anticancer molecular action, toxicity and novel drug delivery systems. *Journal of Pharmacy and Pharmacology*, 65(2):157–170, February 2013.

VITA

Degrees:

- December (expected) 2018 – M.S. in Physics (Biophysics Concentration), Texas Christian University, TX
- May 2016 – B.S. Utica College, NY

Awards and Honors:

- 2017 – Best Poster Presentation, American Physical Society Meeting
- 2017 – Best Interdisciplinary Applications in Contempory Science and Engineering, Texas Applied Mathematics and Engineering Symposium
- 2015 – Top Student Poster Presentation Award, Utica College Student Research Day

Research Experience:

- 2016 - Present – Masters Research, Texas Christian University, TX
- 2014 – Summer Research Experience for Undergrads, Texas Christian University, TX
  "How bad is it doc? The varying predictions of ODE cancer growth models"

Teaching Experience: Teaching Assistant

- Spring 2018 – Two sections of Physics II Lab, TCU
- Fall 2017 – Two sections of Astronomy Lab, TCU
- Summer 2017 – Two sections of Physics I Lab, TCU
- Spring 2017 – Two sections of Archaeoastronomy Lab, TCU
- Fall 2016 – Two sections of Physics I Lab, TCU

Refereed Publications:

- "Differences in predictions of ODE models of tumor growth: A cautionary example", **H. Murphy**, H. Jaafari, H.M. Dobrovolny 2016, BMC Cancer, 16(1):163

ABSTRACT

UNDERSTANDING THE EFFECT OF MEASUREMENT TIME ON DRUG CHARACTERIZATION

by Hope E Murphy, M.S., 2018
Department of Physics and Astronomy
Texas Christian University

Research Advisor: Dr. Hana M. Dobrovolny, Associate Professor of Biophysics

In order to determine correct dosage of chemotherapy drugs, the effect of the drug must be properly quantified. There are two important values that characterize the effect of the drug: $\varepsilon_{\max}$ is the maximum possible effect from a drug, and IC_{50} is the drug concentration where the effect diminishes by half. We use mathematical models to estimate how the values depend on measurement time and model choice. Improper choice of growth model is problematic and can lead to differences in predictions of treatment outcomes for patients. This work intends to understand how choice of model and measurement time affects the relative drug effect and causes the differences in predictions for the most effective dose of anticancer drug for a patient. This work determines the correct doses before trying those in patients to get the most effective therapeutic treatment.